Soil Dynamics and Earthquake Engineering 11 (1992) 27–61

Seismic analysis and design of rockfill dams: state-of-the-art*

G. Gazetas

&

P. Dakoulas

(Received 6 May 1991; accepted 19 July 1991)

Theoretical methods for estimating the dynamic response and predicting the performance of modern rockfill dams subjected to strong earthquake shaking are reviewed. The focus is on methods accounting for nonlinear material behavior, for 3-dimensional canyon geometry, and asynchronous base excitation. It is shown that both strong nonlinearities and lack of coherence in the seismic excitation tend to reduce the magnitude of the deleterious 'whip-lash' effect computed for tall dams built in rigid narrow canyons. Particular emphasis is accorded to Concrete-Faced-Rockfill dams and a case study involving an actually designed dam in a narrow canyon points to potential problems and suggests desirable modifications. In the light of theoretical results, the paper concludes with a discussion on design rules and defensive measures that would lead to robust design schemes of Earth-Core and Concrete-Faced Rockfill dams. Field verification through records of seismic response is, however, a pre-requisite for the confident adoption of such measures in practice.

1 INTRODUCTION – DEVELOPMENTS SINCE 1985

This paper reviews theoretical methods of analysis and discusses issues associated with the design of *rockfill* dams against strong seismic shaking. It could be considered as a continuation of the review paper presented at the 2nd International Conference on Soil Dynamics and Earthquake Engineering, on June 1985, and published in this journal.[58] In that paper a fairly comprehensive exposition of methods of response analysis was given, while particular emphasis was accorded to demonstrating the effects: (i) of inhomogeneity due to dependence of material stiffness on confining pressure; (ii) of 3D canyon geometry; and (iii) of nonlinear and inelastic material behavior.

The focus of the present paper is on two new (post-1985) important developments: (a) the first few 3D solutions have appeared on the effects of 'asynchronous' excitation, arising from oblique plane *SH* waves impinging on the dam-canyon interface; and (b) interest on the seismic behavior of Concrete-Faced Rockfill (CFR) dams has led to a number of investigations on their potential seismic performance. Exposition of these two subjects is given in Sections 4 and 5, and constitutes the bulk of the paper. It is felt necessary, however, that two additional sections, 2 and 3, offer background information by outlining developments (before and after 1985) on the subjects of inelastic response and 3D canyon effects under 'synchronous' (rigid-base) excitation. Moreover, since this paper addresses issues related to the overall seismic performance of dams (as opposed to seismic response analysis that was the sole theme of the previous report), a final section, No. 6, is devoted to design aspects of Earth-Core and, especially, Concrete-Faced Rockfill dams; the emphasis is on defensive measures based on both engineering judgement and theoretical results using state-of-the-art methods of analysis.

Theoretical results presented in the sequel are applicable primarily to *modern rockfill* dams, for the seismic performance and safety of which material degradation due to porewater pressure buildup will not be a significant factor. Hence, liquefaction is not one of the foreseen

*Keynote Lecture presented at the Second International Conference on Recent Advances in Geotechnical Earthquake Engineering & Soil Dynamics, St. Louis, March 11–15, 1991.

Soil Dynamics and Earthquake Engineering 0267-7261/92/$05.00

modes of failure. Instead, permanent deformations, cracking, and other types of local failures are of concern, as they endanger the serviceability of the facilities. Comprehensive reviews of the state of the art on seismic analysis of embankment dams against liquefaction-type failures, have been presented by Seed,[142] Finn,[47,48] and Marcuson, Hynes, & Franklin.[95]

2 INELASTIC RESPONSE TO STRONG SHAKING

To make a realistic prediction of the response of a rockfill dam built in a fairly rigid canyon and subjected to earthquake shaking, careful consideration must be given to the potential effects of the following major phenomena/factors:

(a) nonlinear-inelastic material behavior of rockfill
(b) dependence of rockfill stiffness on confining pressure
(c) 3D canyon geometry
(d) flexibility of supporting canyon and presence of underlying alluvia
(e) wave composition and degree of 'coherence' of the seismic excitation.

Depending on the particular situation, one or more of these phenomena may have an appreciable influence on the response of the dam and will thereby dictate the proper method of analysis. Comprehensive numerical procedures which could rationally simulate all of the foregoing phenomena, while in principle feasible, would be prohibitively expensive at the present time, if they are available.

It appears that the magnitude of nonlinearities is the single major factor in deciding which phenomena to attempt to simulate in the analysis and with what degree of sophistication. Whenever nonlinearities are unimportant as may be the case with stiff modern dams subjected to shaking having peak ground accelerations (pga) of the order of 0·2 g or less, it seems that all the other listed three factors, i.e. (b), (c), (d) and (e), should be properly modeled. Note, however, that some of the effects of factors (b) and (c) may be counterbalanced by the effect of factors (d) and (e). Indeed, as the degree of inhomogeneity (due to dependence of stiffness on confining pressure) increases and as the canyon becomes narrower a 'whip-lash' effect tends to occur; as a result, high absolute accelerations and high shearing deformations tend to develop at the topmost quarter of the dam.[58] On the other hand, as it will be seen in Section 4 herein, when the excitation is assumed to consist of plane obliquely-incident *SH* waves, rather than assuming a fictitious 'rigid-base' motion, destructive wave interference phenomena may lead to reduced midcrest acceleration, in function of the velocity contrast between dam and canyon.

A preliminary assessment of the importance of each of these three factors, (b), (c), (d) and (e), using simple analysis procedures such as some of those described in this paper and in Gazetas,[58] is a first step before embarking into comprehensive sophisticated numerical computations. When designing against very strong potential shaking, during which the dam is expected to respond in a highly nonlinear fashion, the other listed phenomena may lose some of their importance, as it will be shown in the sequel.

2.1 Outline of nonlinear methods of analysis

'Equivalent Linear' Method.[76] An equivalent linear analysis is performed in an iterative way. A set of moduli and damping ratios is initially assumed and a series of linear analyses is conducted, with each calculation using soil moduli and damping ratios compatible with the levels of shear strain calculated in the previous step. To select modulus and damping ratio for each iteration, an 'equivalent' effective strain amplitude is estimated as a fraction (usually 2/3) of the peak shear strains.

The method is empirical and its convergence to the 'correct' answer has not been proven, even though in most practical problems convergence is achieved at most in five iterations.

For moderately strong levels of shaking the peak response values seem reasonable, while the response to very strong excitation may be overestimated (the usual case) or even underestimated. By themselves, peak values do not contain information about how strong or how weak the rest of the stress on strain history is. Therefore, it is not impossible for the method to lead to an artificially over-damped and over-softened system; or in case of relative uniform motion to underestimate both damping and softening. Consequently, the method may not reproduce adequately the details of the response history.

Since the method is essentially linear, it is possible that one of the predominant frequencies of the excitation may coincide with one of the natural frequencies of the dam, and therefore there is a tendency for spurious resonances to develop. Finally, the method can not provide information on permanent displacements and deformations, and needs to be complemented by separate, semi-empirical, procedures for assessing residual and sliding displacements.[89,111]

In 2D and 3D analyses, the equivalent linear method must define the variation with maximum shear strain amplitude of another soil parameter, in addition to shear modulus. In some formulations it is the Young's modulus which decreases with increasing strain in proportion to shear modulus; consequently, it is the bulk modulus which decreases with increasing shearing, a questionable assumption for undrained loading conditions. In other formulations it is the Poisson's ratio which varies with shear strain, with bulk modulus kept constant.

'Simplified Nonlinear' Method.[58] This approximate nonlinear (but essentially elastic) method attempts to overcome in a simple way the two main limitations of 'equivalent linear' procedures: the arbitrary definition of the 'equivalent' shear strain amplitude and the 'spurious resonance' effect. The basic premise of the method is that soil moduli and damping ratios can be updated at various time intervals so as to be consistent with the root-mean-squared (rms) values, $\gamma_{rms}(t)$, of the shear strain during the same interval. In other words, updating of the soil parameters is enforced at several points along the time axis, in contrast with the single, after-the-analysis updating of the 'equivalent linear' scheme.

The numerical analysis is performed in two consecutive phases. The first phase aims at obtaining an estimate of the time history of the rms shear strain, $\gamma_{rms}(t)$; the second phase computes the dam response through piecewise linear analysis in small time steps. The equivalent sinusoidal shear strain amplitude γ_e, corresponding to γ_{rms} is found by equating *shear strain energies* of the actual and a sinusoidal motion:

$$\gamma_e = \sqrt{2}\gamma_{rms} \tag{1}$$

These γ_e values are used to update moduli and damping ratios. The specific details of each phase can be found in Refs 29 and 58.

Comparison of typical response histories computed by Simplified Nonlinear analysis of a shear-beam dam model and by equivalent linear analysis of a finite-element dam model, reveals the general accord of the methods and shows that while the former can preserve some of the high frequency components of the motion, as is appropriate, the 'equivalent linear' finite-element analysis filters out some of these frequencies.

'Hysteretic Galerkin' formulation.[127,128] This more rigorous (but still simplified) method for determining the nonlinear *inelastic* response of earth dams is based on a Galerkin formulation of the equations of motion in which the solution is expanded using *basis functions* defined over the whole dam. 1D, 2D, and 3D geometries can be handled with the method. It is found convenient to use as basis functions the eigenmodes of the linearized homogeneous dam. The hysteretic stress-strain behavior of the soil is modeled by using elastic-plastic constitutive relations based on multisurface kinematic plasticity theory. The semi-discrete coupled nonlinear ordinary differential equations are solved through step-by-step integration using Newmark's algorithm and Newton-Raphson type interations.

The method has been applied to 1D models, with the linear homogeneous shear-beam mode shapes as basis functions; 2D models, along with the rectangular homogeneous shear-wedge shapes; and in three dimensions along with the Abdel-Ghaffar & Koh[7] method for non-homogeneous dams in rigid rectangular, trapezoidal or triangular canyons.

In recent years the method has been further extended by Elgamal[40] and Yiangos & Prevost[172] to account for soil degradation due to porewater pressure generation. The latter authors study a uniform homogeneous earthfill dam section, modeling the soil as a two-phase poro-elastoplastic material with fully coupled soil skeleton and pore pressure equations in the saturated portion of the dam.

'Layered Inelastic Shear-Beam' (LISB) method. This method attempts to combine the simplicity and efficiency of the one-dimesional shear-beam type of analysis with the versatility of (plane-strain) finite-element in handling zones of different material and nonlinear element behavior. The method involves two stages. In stage I, the dam is discretized into finite elements and is subjected to horizontal static inertia-like forces. The nonlinear deformations of the dam are computed using the best available plane-strain code, while the applied horizontal forces are gradually increased until large enough strains develop in most elements of the dam. This static analysis provides for each horizontal layer (super-element) the backbone curve relating the total horizontal shear force and average horizontal layer distortion; this backbone curve together with the extended Massing criterion provides the complete hysteretic constitutive relation required for the dynamic analysis in stage II. In the second stage the dam is discretized as a one-dimensional layered triangular shear-beam and the dynamic response of the dam is computed using nonlinear shear-beam formulations.

The method has been successfully tested against equivalent-linear and plasticity-based finite-element analyses, and is capable of estimating '*local*' (element) acceleration, stress, and strain histories from the corresponding '*layer*' (super-element) histories that are directly computed in the shear-beam analysis of stage-II.

Approximate 2D nonlinear effective-stress analysis.[46,47] This method extends the 1D hyperbolic-massing model of cyclic behavior in simple shear to approximately account for inelastic soil behavior in two dimensions. The method can handle transient and residual porewater pressures generated and diffused during the shaking, as well as volumetric compaction due to shear. The model for residual porewater pressures (which arise due to plastic deformations) is a straightforward extension of the 1D Martin-Finn-Seed[96] model that has been widely used for site-amplification and liquefaction studies. Applications of this method have been published for embankments and related earth structures. Tested against centrifuge-measured seismic histories of deformations and residual porewater pressures the method seems capable of capturing all the important features of the response with very good engineering accuracy and,

according to Finn,[47] at a substantially-reduced computational cost in comparison with more rigorous plasticity-based models.

Rigorous Plasticity-Based FE and FD Methods.[79,127,172,173] These methods utilize plasticity models of soil behavior in a FE formulation. For example, Prevost and co-workers discretize the dam in eight-node isoparametric 'brick' elements or four-node isoparametric elements for three and two dimensions, respectively. The formulation can handle either one of the three orthogonal components of the seismic excitation (upstream-downstream, vertical, longitudinal). The hysteric stress-strain behavior of the dam material is modeled by using multisurface kinematic plasticity theory, which along with a symmetric backbone curve generates a Massing-style hysteretic behavior. The time integration of the semi-discrete finite element equations is performed by an implicit-explicit predictor-multicorrector algorithm, based on the Newmark method. The general validity of the method has been checked against the recorded response of the Santa Felicia[128] and of the Long Valley dam.[62] Both 2D and 3D analyses were performed in these studies. However, the finite-element *mesh* used in such analyses seems to be very coarse, especially in 3D studies, due to the very substantial computational requirements of the method (e.g. solution time in an IBM 370/3082 exceeding four hours). It is quite likely that high frequency components are artificially filtered out or at least reduced as they propagate through a coarse mesh; this may especially affect the accelerations computed for the crest zone.

2.2 Main results and conclusions

Some conclusions of particular practical significance, drawn from parametric investigations with the outlined nonlinear methods of analysis are discussed herein.

For dams built in long canyons and modeled as plane triangular-wedge structures, development of strongly-nonlinear response affects in a beneficial way the accelerations experienced at the top of the dam. Figure 1 elucidates this influence of material nonlinearity and compares it with the influence of material inhomogeneity. The figure refers to a hypothetical tall dam having an average low-strain S-wave velocity $V_{s,\max} = 360$ m/s, and subjected to the Taft Lincoln School Tunnel record, scaled at pga = 0·40 g. The dam is modeled as (i) a linear and (ii) a nonlinear shear beam, the initial shear modulus ($G_{\max}$) and the shear strength (τ_{ult}) of which are taken to increase in proportion to z^m, where z = depth from crest; m is parametrically varied from 0 (homogeneous dam), to 1/3 and to 2/3 (inhomogeneous dams). In all cases $V_{s,\max}$ remains the same. The average-stress–average-strain backbone relationship for each horizontal layer, i.e. across the width of the dam is assumed to be hypebolic:

$$\tau = \tau(z, \gamma) = G_{\max}(z) \frac{\gamma}{1 + \gamma/\gamma_r} \qquad (2)$$

where γ_r = the reference strain = $\tau_{ult}(z)/G_{\max}(z)$. For a *constant* value $\gamma_r = 0{\cdot}003$ the resulting average $\tau - \gamma$ curve is plotted in Fig. 1, and is chosen so that the dam experiences mildly and strongly inelastic response, respectively, when subjected to the aforesaid scaled Taft record.

It is pointed out that use of such semi-realistic nonlinear dam models does not necessarily imply their endorsement for general use; it has rather been motivated by the fact that they can be defined with only three parameters: the average value of low-strain modulus $G_{\max}$, the inhomogeneity parameter m, and the reference strain γ_r.

Figure 1 contrasts the distributions of peak values of absolute acceleration and shear strain from the 'consistent' linear ($V_s = 280$ m/s) and nonlinear ($\gamma_r = 0{\cdot}003$) analyses. Several trends are worthy of note. First, for all types of inhomogeneity ($m = 0$, 1/3, 2/3) strong nonlinear action leads to substantially reduced amplification. Peak crest accelerations decrease on the average from about 1·50 g during linear oscillations — amplification of 3·75 — to barely 0·50 g during strongly inelastic shaking: an amplification of merely 1·25. On the other hand, despite the inelastic action during the two nonlinear analyses (or perhaps because of it), the distributions of peak shear strains essentially retain their linear-elastic shape.

There are three main causes for the tendency of peak accelerations to decrease with increasing degree of material nonlinearity: (i) increased hysteretic dissipation of wave energy, (ii) destruction of potential resonances, and (iii) cutting-off accelerations associated with shear stresses exceeding the ultimate material resistance, τ_{ult}. Particularly vulnerable are the high-frequency high-amplitude acceleration components which tend to develop in inhomogeneous dams.

It is reasonable to expect that the similar high-frequency high-amplitude near-crest acceleration components experienced by dams built in narrow canyons would be similarly depressed during strong inelastic action. A first piece of tentative analytical evidence that this is indeed the case has been provided by Prevost *et al.*[127] Using a 3D finite-element model based on a multisurface kinematic plasticity theory, they computed (with the help of an admittedly rather coarse 3D mesh) the crest accelerations of the Santa Felicia dam, subjected to two excitations: (i) the lateral motion recorded near the outlet works of the same dam during the 1971 San Fernando Earthquake (duration: 35 sec, peak acceleration: 0·22 g); and (ii) the Pacoima Dam Abutment record (duration used: 15 sec, peak acceleration: 1·20 g); Table 1 compares the peak crest accelerations computed for a compatible 2D model of the mid-cross-section and from the 3D analyses. The latter predict lower values, in both cases, with the discrepancy increasing considerably with the intensity of excitation. Although it is likely that some high-frequency (low wavelength) components are artificially filtered out by the coarse

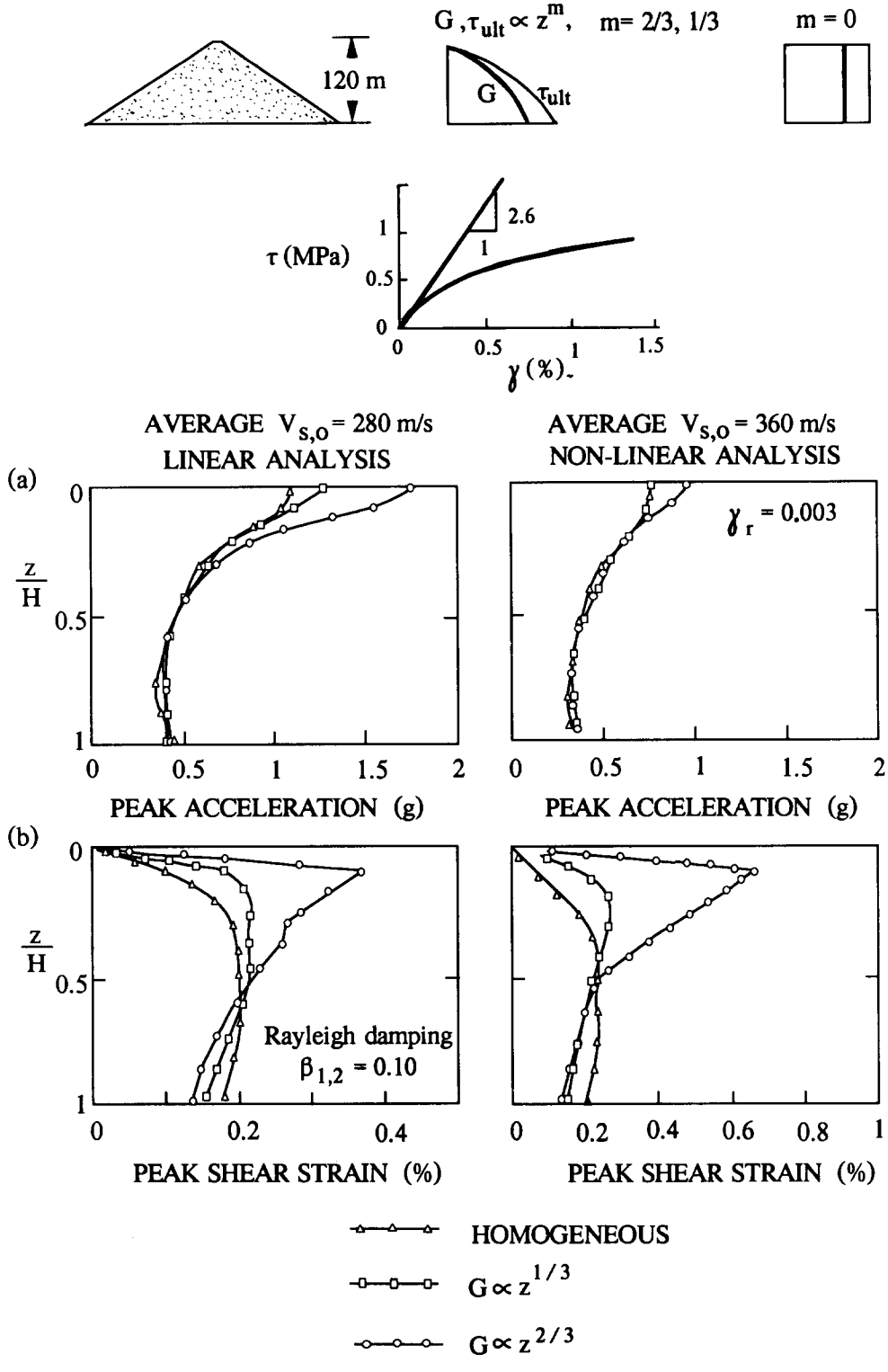

Fig. 1. For a given excitation, with increasing nonlinear inelastic action: (a) the near-crest peak accelerations decrease and the effects of inhomogeneity tend to diminish; but (b) the peak shear strain distributions remain nearly unchanged, both in magnitude and shape.

mesh, these results are qualitatively consistent with the trends noted in Fig. 1 (nonlinearity versus inhomomeneity). Hence, it is more than a mere suspicion that soil nonlinearity may tend to suppress reduction of the adverse effects of narrow canyon geometries on mid-crest accelerations.

3 3D CANYON EFFECTS UNDER 'SYNCHRONOUS' BASE EXCITATION

3.1 Outline of methods of analysis

The assumption of plane-strain conditions (which forms

Table 1. Inelastic 2D versus 3D peak crest acceleration for Santa Felicia Dam[127]

Excitation Record	Inelastic 2D Prediction	Inelastic 3D Prediction
Santa Felicia 1971	0·26 g	0·22 g
Pacoima, 1971	0·86 g	0·58 g

the basis of the 2D codes which in most cases are used in practice) is exactly valid only for infinitely long dams subjected to a 'synchronous' base excitation (i.e., identical motion of all points along the base). For dams built in narrow valleys, as is often the case with rockfill dams, the presence of relatively rigid abutments creates a three-dimensional (3D) stiffening effect, whereby natural periods decrease and near crest accelerations increase sharply as the canyon becomes narrower.

In the last ten years or so a number of formulations have been published for the seismic response analysis of 3D dam-canyon systems under rigid-base ('synchronous') excitation. Numerical results have been published for several idealized soil profiles (sketched in Fig. 2) as well as for some actual geometries. The vast majority of these methods and results refer to linear analyses, but attempts for 3D inelastic solutions (a truly formidable problem) have also been reported.[62] See the 1985 review paper[58] for detailed exposition of 3D methods and results. Only an outline of methods is given herein. Specifically:

- For dams having a plane of symmetry perpendicular to the longitudinal axis Martinez & Bielak have developed a numerical procedure which overcomes the expense of 3D finite-element analyses. To this end, they neglect the (indeed secondary) longitudinal deformation and discretize in finite elements only the dam midsection, which coincides with the plane of symmetry. Displacements and inertia forces are expanded in Fourier series (of m terms) in the longitudinal direction and the problem is reduced to solving m uncoupled 2D finite elements problems, where a small number ($m \approx 4$–5) of longitudinal modes suffices.
- An approximate formulation based on the shear-beam concept, in which longitudinal and vertical displacements are ignored but no symmetry is required, has been developed by Ohmachi.[113,114] The dam is divided into super-elements through vertical, closely-spaced transverse planes. Each super-element has the shape of a truncated pyramid the bases of which are two neighboring cross-sections and which are assumed to behave as triangular shear beams. A linear interpolation function is used to express the displacement shape in the longitudinal direction and, by enforcing compatibility of deformation between super-elements, the solution is obtained in the form of natural frequencies and modal shapes. Ohmachi's results for rectangular, trapezoidal and triangular canyons confirm the significance of canyon geometry

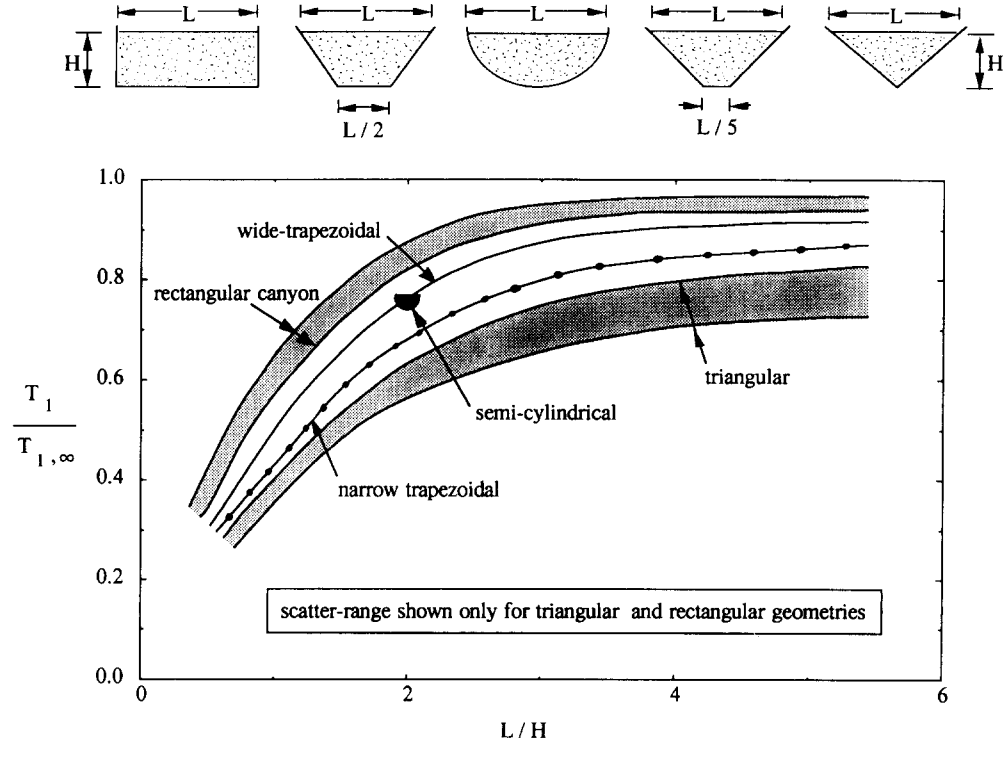

Fig. 2. Effect of canyon geometry on the fundamental natural period.

found by Martinez & Bielak, although some quantitative differences exist between the natural frequencies reported in the two studies with triangular canyons. Of particular interest is the successful use of this approximate 3D shear-beam model, in conjunction with an average-across-the-width shear modulus proportional to $z^{2/3}$, to reproduce the results of full-scale force-vibration tests on Bouquet Dam.

- Abdel-Ghaffar & Koh[5,6] have presented a semi-analytical solution for dams built in canyons of any shape but having a plane of symmetry. This solution is based on the Rayleigh-Ritz method with the shear-beam model shapes or even simple sinusoids as 'basis functions', and involves an appropriate transformation of the dam geometry into a cuboid. Results have been presented for natural frequencies and mode shapes of an inhomogeneous dam in a trapezoidal canyon, and an attempt has been made to reproduce the recorded seismic response of the Santa Felicia Dam during the 1971 San Fernando Earthquake. Only a limited number of results have been presented. But the method is versatile and could be used for an approximate solution of the nonlinear problem.[39]
- A special 3D dynamic finite-element formulation has been developed by Makdisi *et al.*[90] by replacing the 2D plane-strain isoparametric elements of the computer code 'Lush' with prismatic longitudinal elements having six faces and eight nodal points. To reduce computer storage and time requirements, the (secondary) longitudinal displacements can be ignored and only shear waves propagate vertically and horizontally in the embankment. Results have been presented for steady-state and transient response of homogeneous dams in triangular canyons. Subsequent work at Berkeley[101,102] has avoided the foregoing simplifying restriction on longitudinal deformations. The method has been used to backfigure the dynamic stiffness characteristics of the Oroville Dam using its recorded response to the August 1975 Oroville Earthquakes; the estimated value of $K_{2,\max} = 170$ is in reasonable agreement with laboratory test results on material from the shell of the dam.
- Analytical closed-form solutions are particularly valuable even if the canyon shapes are highly idealized. Hatanaka[69] and Ambraseys[10,11] presented solutions for a rectangular canyon, while more recently a simple closed-form analytical solution has been derived by Dakoulas & Gazetas for the dynamic lateral response of a homogeneous earth dam built in a semi-cylindrical canyon (Fig. 2). These solutions are based on a generalization of the shear-beam concept. Only lateral displacements and shear deformations are allowed, and they are assumed to be uniformly distributed across the dam, i.e. independent of y (see, e.g. Fig. 6). With these assumptions, the solution is exact; no other approximation is introduced such as, for example, the assumption of independent vertical and horizontal distributions of mode shapes in the aforementioned formulation of Ohmachi.[113] The results are in the form of especially simple algebraic expressions for natural periods, modal shapes, steady-state transfer functions, and participation factors for transient seismic excitation. Table 2 depicts these expressions and compares them with those for a (homogeneous) 1D shear beam and a homogeneous 2D shear beam in a rectangular canyon. Also given in this table for direct comparison are (i) the formulae corresponding to an inhomogeneous 1D shear-beam with modulus proportional to $z^{2/3}$; and (ii) approximate formulae for the 3D natural frequencies of a homogeneous dam in a rectangular canyon.

Finally recall that the (already presented in 2) formulation by Prevost *et al.*[127,128] in which a kinematic multi-yield-surface plasticity constitutive relation for soil is used in F.E. modeling of 3D dams in arbitrarily-shaped canyon. Also, new justified attempts for simplified 3D solutions are described, among others, in Prato[124] and Hirata & Shinozuka.[71]

3.2 Characteristic results

The significant 3D canyon effects that have emerged from theoretical studies using the preceding methods are summarized herein with the help of Figs 2, and 3. (See Gazetas[58] and the original papers for more detailed information.) Specifically:

a. Figure 2 illustrates the stiffening effect of narrow canyon geometries on the fundamental natural period, $T_1 = T_1(L/H)$, of a dam for the five different canyon shapes. Both shear-beam and finite-element based results are shown in this figure. (Note that $T_{1,\infty}$ is hardly influenced by inhomogeneity and that the ratio $T_1/T_{1,\infty}$ is essentially the same for shear-beam and finite-element idealizations; in other words, while shear-beam formulations usually underestimate $T_{1,\infty}$ by about 5%–10%, they also tend to underestimate $T_1(L/H)$ by approximately the same amount.) Evidently, the various outlined formulations produce consistent results.

b. Figure 3 depicts the effects of narrow canyon geometry on the steady-state response of a dam to a harmonic rigid-base excitation, $u_g \exp(i\omega t)$. Analytical expressions for the crest amplification functions (AF) are shown in Table 2 for a semi-cylindrical canyon, and for a rectangular canyon with L/H = 2. In the figure, the midcrest 'rigid-rock' AF for a dam in a semi-cylindrical canyon is compared with the one obtained from a 1D shear-beam analysis for the midsection of the dam. It is evident that, in addition to predicting lower natural frequencies, the plane model underpredicts both the amplification at first resonance and the relative importance of higher resonances. The effect of different canyon shapes,

Table 2. Analytical expressions forsome 2-D and 3-D earth dam models

Earth dam model	Fundamental period T_1	Ratio of natural periods T_1/T_2	nth Natural circular frequency ω_n	nth Modal displacement $U_n(x = 0, z)$	nth Mode participation factor $\lvert P_n \rvert$	Steady-state midcrest/base transfer ('amplification') function $AF = [\tilde{u}(z = 0) + \tilde{u}_g]/\tilde{u}_g$	
						I. 'Rigid-rock' amplification	II. 'Elastic-rock' amplification
Homogeneous 1-D shear-beam	$2{\cdot}61\,\frac{H}{V}$	2·3	$\beta_n \frac{V}{H}$	$J_0(\beta_n\zeta)$	$\frac{2}{\beta_n J_1(\beta_n)}$	$\frac{1}{J_0(a_0)}$	$\frac{1}{J_0(a_0) + i\alpha J_1(a_0)}$
Inhomogeneous 1-D shear-beam $G \sim z^{2/3}$	$2{\cdot}57\,\frac{H}{\bar{V}}$	2	$\frac{7}{9} n\pi \frac{\bar{V}}{H}$	$\zeta^{-2/3} \sin[n\pi(1 - \zeta^{2/3})]$	$\frac{2}{n\pi}$	$\frac{a_0}{\sin a_0}$	$\frac{a_0}{\sin a_0 + i\alpha\left(\frac{\sin a_0}{a_0} - \cos a_0\right)}$
Homogeneous shear-beam in semi-cylindrical canyon	$2\,\frac{H}{V}$	2	$n\pi \frac{V}{H}$	$\frac{\sin(n\pi\zeta)}{n\pi\zeta}$	2	$\frac{a_0}{\sin a_0}$	$\frac{a_0}{\sin a_0 + i\alpha\left(\frac{\sin a_0}{a_0} - \cos a_0\right)}$
Homogeneous shear-beam in rectangular canyon with $L/H = 2$	$2{\cdot}19\,\frac{H}{V}$	2	$\left(\beta_n^2 + \frac{\pi^2}{4} r^2\right)^{1/2} \frac{V}{H}$	$J_0(\beta_n\zeta) \sin(r\pi\zeta/2)$	$\frac{8}{\pi\beta_n J_1(\beta_n)}$	$1 + \frac{4}{\pi} \sum_{r=1}^{\infty} \sum_{n=1}^{\infty} \frac{[1 - (-1)^r]a_0^2}{r\beta_n J_1(\beta_n^2)(\beta_n^2 + r^2\pi^2/4 - a_0^2)}$	*
Homogeneous shear-beam in rectangular canyon with $L/H = 2$ a uniform layer $h/H = 0{\cdot}25$ and the same wave velocity	$2{\cdot}57\,\frac{H}{V}$	1·89	$\left(b_n^2 + \frac{\pi^2}{4} r^2\right)^{1/2} \frac{V}{H}$	$j_0(b_n\zeta) \sin(r\pi\eta/2)$, $0 < \zeta < 1$ $J_0(b_n) \sin[b_n(1{\cdot}25 - \zeta)]$ $\sin(r\pi\eta/2)/\sin(b_n/4)$, $1 < \zeta < 1{\cdot}25$	$\frac{32 \cos(b_n/4)}{r\pi J_1(b_n)[5b_n - 2\sin(b_n/2)]}$	*	*
Approx. 3-D model of homogeneous dam in rectangular with $L/H = 2$ [97]							
(i) steep slope $B/H = 1{\cdot}5$	$2{\cdot}37\,\frac{H}{V}$	1·80	$\left(\delta_n^2 + \frac{\pi^2}{4} r^2\right)^{1/2} \frac{V}{H}$	*	*	*	*
(ii) flat slope $B/H = 3{\cdot}0$	$2{\cdot}51\,\frac{H}{V}$	1·82					

Notation:
- β_n = nth root of $J_0(\beta) = 0$; for example: $\beta_1 = 2{\cdot}40$, $\beta_2 = 5{\cdot}52$, $\beta_3 = 8{\cdot}65$ and so on.
- δ_n = nth eigenvalue of the 2-D plane-strain problem, δ_n = function of slope B/H; $\delta_n \leqslant \beta_n$; for example: $\delta_1 \approx 2{\cdot}15$ for $B/H = 1{\cdot}5$.
- b_n = nth root of $\tan(b_n/4) = J_0(b_n/J_1(b_n)$, $b_1 = 1{\cdot}88$, $b_2 = 4{\cdot}34$, $b_3 = 6{\cdot}87$, . . . ; $r = 1, 2, 3, \ldots$
- $\zeta = z/H$ = normalized depth, $\eta = x/H$ = normalized horizontal coordinate.
- $\ddot{u}$ = midcrest acceleration relative to base.
- $a_0 = \omega H/V$, in which V is the average shear wave velocity of the dam.
- α = impedance ratio = $(\rho V)_{\text{dam}}/(\rho V)_{\text{canyon}}$.
- $i = \sqrt{(-1)}$.

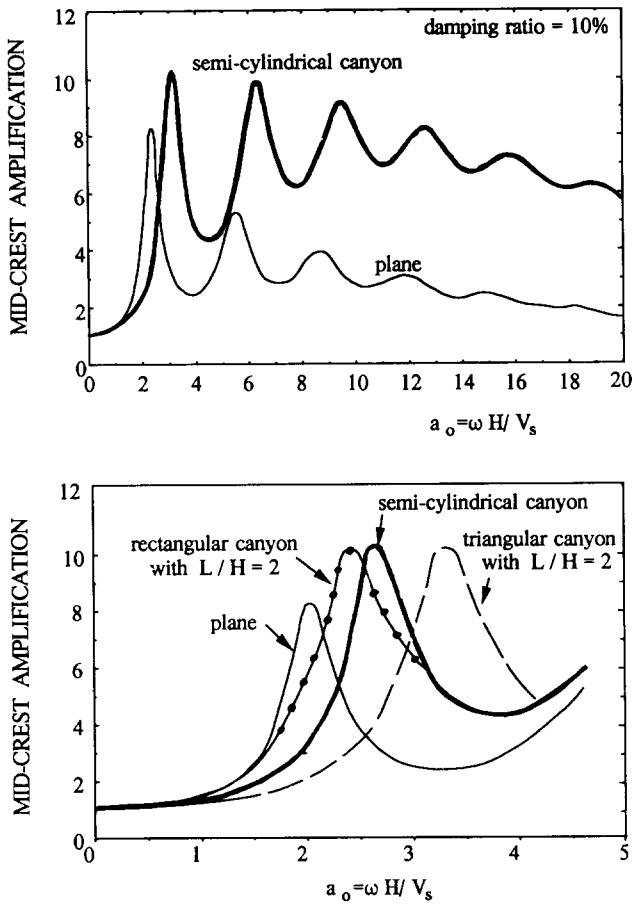

Fig. 3. Steady-state response to harmonic base excitation: (a) semi-cylindrical dam determined from 3-dimensional and from plane shear-beam analysis; (b) effect of canyon shape on midcrest amplification function.

having aspect ratio $L/H = 2$, exhibits a consistent trend and reveals that the value of AF at first resonance, AF_{max}, is practically independent of the exact canyon shape; for the considered value of the hysteretic damping ratio, $\beta = 0{\cdot}10$, $AF_{max} \approx 10$. Moreover, in triangular valleys, $AF_{max} \approx 10$ for all values of the aspect ratio L/H.

An interesting case history which provides field evidence in support of the results of Fig. 3 has been recently published by Mejia *et al.*[103] It relates to the Ririe Dam, in Idaho, a 76 m high earth-core rockfill dam built in a relatively narrow canyon. The plan of the dam suggests a nearly triangular canyon shape with an 'effective' aspect ratio L/H of about 3. The dam was shaken by the 1983 Mt. Borah earthquake ($M_L = 6{\cdot}9, r \approx 180$ km) which triggered accelerographs at one of the abutments and at mid-crest. The amplification ratio between the Fourier spectra of the crest and the abutment acceleration records is plotted versus frequency (in logarithmic scale) in Fig. 4. The theoretical curve also plotted was computed by Mejia *et al.*[103] from a 2D, finite-element model, the properties of which, however, were selected so that, essentially, the fundamental frequency and amplitude of their model would match the corresponding

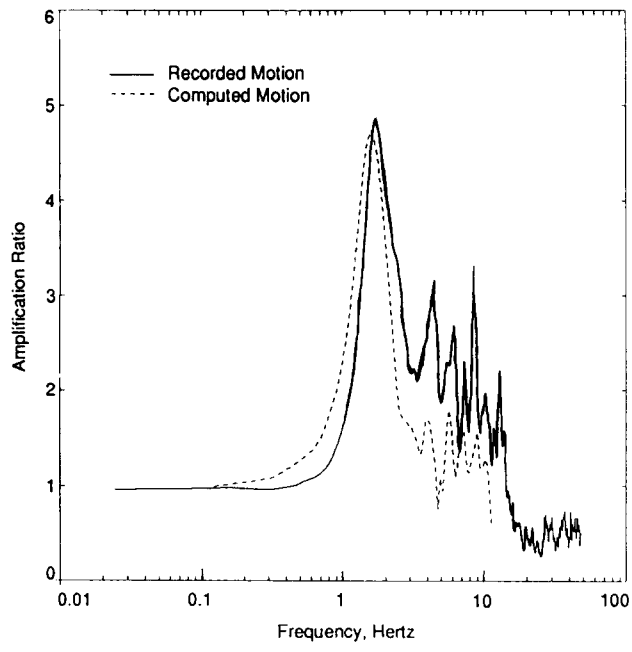

Fig. 4. Crest-to-abutment amplification spectrum of the Ririe Dam in the 1983 Mt. Borah earthquake. The theoretical spectrum (dotted line) was computed with a 2D plane-strain model, in which the moduli were selected to account for the apparent 'stiffening' effect of the narrow canyon. From Mejia *et al.* 1991.

values of a (more appropriate) 3D model. Notice that despite this matching at the fundamental frequency, the higher-mode amplitudes of the 3D reality exceed those of the 2D analysis in a way similar to that suggested by the theoretical 3D-versus-2D plot of Fig. 3.

c. The foregoing differences between 2D and 3D steady-state amplification functions are echoed in the response accelerations predicted for dams in ∞-long and in narrow canyons. Peak accelerations near the crest of dams in narrow canyons ($L/H \approx 2$) may exceed by a factor of 2 the corresponding plane-strain values — an apparent 'whip-lash' effect due to wave 'focusing'.[58] Moreover, 3D acceleration histories are much richer in high-frequency components of motion, since: (i) the 3D fundamental frequency exceeds by 30%–50% the plane-strain $f_{1\infty}$; and (ii) the importance of the higher harmonics is much stronger in the 3D case, as already discussed.

The consequences of these very substantial effects of a narrow canyon geometry are further discussed herein with the help of a case study involving a CFR dam (Section 5).

4 3D CANYON EFFECTS UNDER SEISMIC WAVE ('ASYNCHRONOUS') EXCITATION

The discussed 3D studies of the seismic response of dams have invariably assumed that the points at the dam-valley interface experience identical and synchronous

(in-phase) oscillations and hence that a single accelerogram suffices to describe the excitation. In reality, however, seismic shaking is the result of a multitude of body and surface waves striking at various angles and creating reflection and diffraction phenomena. The resulting oscillations differ (in phase, amplitude, and perhaps also in frequency characteristics) from point to point along the dam-valley interface. The simplifying assumption of identical and synchronous excitation ('rigid-base motion'), advanced solely for mathematical convenience, may be reasonable only for very low frequencies; at higher frequencies, when the wavelengths of the incident seismic waves become equal to or smaller than the characteristic dimensions of the dam, differences are expected to arise rendering the 'in-phase' hypothesis unrealistic.

In this section dam and canyon are excited solely by harmonic plane *SH* waves impinging at different angles, in the vertical plane of the dam axis. This is clearly an improved but still not complete representation of the seismic environment, as additional factors (i.e. other than wave passage) contribute to the spatial variability of the ground motion at the dam-canyon interface. This additional variability results in incoherent base motion, the effects of which have so far been studied only for shallow foundations (e.g. Veletsos & Tang[164]). Note, however, that the 'wave passage' and 'ground motion incoherence' effects are of a similar nature, with some quantitative rather than qualitative differences. Hence, at this rather early stage of understanding, it is more important to concentrate on developing a better insight of the basic mechanisms and the parameters controlling the response of a dam subjected to asynchronous base motion, than to refine the representation of the spatial variability of the ground excitation.

The difficulty in the theoretical analysis of the dam-canyon system stems mainly from its 3-D geometry. Even with significant simplifications on material behavior, geometry and excitation, analytical solutions are very difficult to obtain, while finite-element methods have inherent difficulties in modeling the associated radiation damping effects and are too costly in representing large 3D structures. Thus, there have been only few isolated attempts to address this problem.[34,109] However, valuable insight to this problem can be obtained from the results of numerical/analytical studies on the effects of geologic and topographic features on seismic motions. Such studies may help us understand the phenomena controlling the response of the dam-canyon system. Thus, it is beneficial to present some of the main conclusions from available studies on the response of (a) canyons of semi-circular or semi-elliptical shape and (b) semi-circular, semi-elliptical, cosine and nearly-rectangular shapes.

4.1 Response of canyons to *SH* waves

The response of a canyon to incident *SH* waves is characterized by amplification at its edges and deamplification at its bottom. Trifunac[161] presented an exact closed-form solution for the response of a semi-cylindrical canyon subjected to *SH* waves, and Wong & Trifunac[170] extended the solution for semi-elliptical canyons. Their results show that for incident waves forming an angle θ with the vertical and traveling from the left to the right of the canyon there is scattering and diffraction of waves predominantly on the left side, while the right edge of the canyon is in a shadow zone. Consequently, the response of the left edge of the canyon experiences higher amplification that the response of the edge in the shadow zone. For incident wave-lengths that are small compared to the size of the canyon, the amplification of surface displacements are as high as 2 for both semi-cylindrical and semi-ellipitcal canyons of all aspect ratios. For an angle $\theta = 90°$ (propagation of *SH* waves along the horizontal direction) and a wide range of frequencies, the left edge transfer function (amplification) varies from 1·7 to 2, while the right edge transfer function (deamplification) varies from 0·3 to 1. Incident and reflected waves interfere at the left side of the canyon to form a standing wave pattern, which is superimposed to the motion propagating to the right. With such an excitation, if the presence of a dam had little effect on the motion at the dam-canyon interface, the amplitude of the excitation at the dam base would be up to 6-7 times larger at the left edge than the one at the right edge for a semi-cylindrical canyon. For a semi-elliptical canyon with depth to width ratio equal to 1, this ratio of amplitudes may reach values as high as 16 to 20, depending on the frequency. Of course, the above amplitude differences are rather an extreme case, since such a high angle of incidence of *SH* waves is of limited practical interest. In addition to the amplitude variation, phase differences are also substantial ranging from 0 to π (or several π), depending on the angle and the frequency of the incident waves, and the geometry of the dam. The phase difference increases with the angle of incidence and the frequency of the motion.

Similar frequency and time domain analysis by Kawase[80] using the Discrete Wavenumber Boundary Element method, confirmed that the constructive interference of incident and reflected waves results in a substantially higher response near the left edge of the canyon. Diffracted waves originate at the edges of the canyon and propagate along the surface of the canyon with the apparent *S* wave velocity. It is interesting that, as shown in the study, time domain analyses can demonstrate in a clearer way the presence of reflected and diffracted waves than a frequency domain analysis. Comparisons between frequency and time domain solutions by Trifunac,[161] Kawase[80] and Wong & Jennings[168] suggest that the effects of canyon geometry may not be as pronounced during short-duration impulse-like shaking.

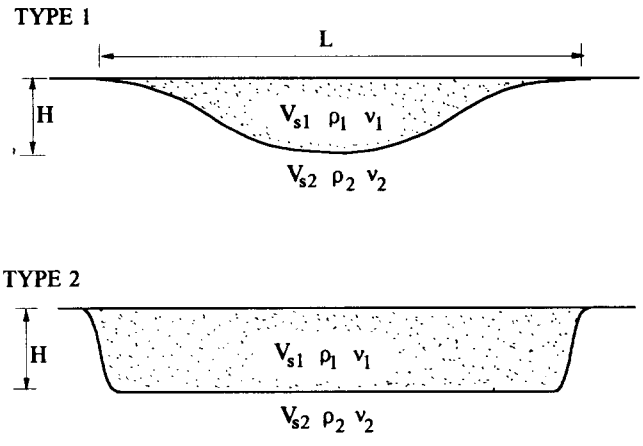

Fig. 5. Geometry of alluvial valleys studied by Bard & Bouchon.[15]

4.2 Response of alluvial valleys to *SH* waves

The presence of an alluvial deposit in the canyon may significantly change the response characteristics along the canyon surface. Among the first to study this problem, Trifunac[162] and Wong & Trifunac[170] presented plane-strain closed-form solutions for the response of an alluvial deposit in semi-cylindrical and semi-elliptical canyons, respectively, to incident plane *SH* waves. The two studies have demonstrated that displacement amplification on the alluvium surface is much larger than on the surface of an empty canyon (where they would not exceed 2) and may change by as much as an order of magnitude within a distance equal to a fraction of the wavelength. Standing waves appear not only in front of the canyon, but also within the alluvial valley. The response depends significantly on the interference of the transmitted waves with their reflections on the alluvium boundaries, which results in the formation of Love waves propagating back and forth within the two edges of the alluvium.

The phenomenon is demonstrated in a comprehensive study by Bard & Bouchon[15] using the Aki-Larner method.[9] Two types of valleys are considered in their study, shown in Fig. 5: Type 1, having a one-cycle cosine shape, which is conducive to wave focusing effects (stronger 3D influence); and Type 2, having a flat bottom confined by steep half-cosine edges, which generates surface waves in a finite-width plane layer (weaker 3-D influence). The time domain response of a type 1 alluvial valley reveals that a wave disturbance is generated at the edge of the valley and propagates horizontally towards the other edge with a characteristic dispersion, in which higher velocities correspond to smaller layer thicknesses and lower frequencies. The reported range of phase velocity values is in agreement with the fundamental Love wave phase velocities for the case of a flat layer with thickness equal to the maximum thickness of the valley. For vertically incident *SH* waves the maximum constructive interference of the waves generated at the two edges of the valley occurs at its center and results in very strong amplification, exceeding 5·5 times the surface amplification on a halfspace. For obliquely incident waves traveling from the left to the right, there is one particular angle of incidence (about 30° for the cases examined) for which the surface amplification becomes maximum. This also appears in the frequency domain studies by Trifunac[162] and Wong & Trifunac,[170] although there is no unique preference angle for all geometries and frequencies. The two investigators explain the occurrence of the high amplitude as the result of wave focusing, created by the transmission of waves through the curved surface of the alluvium-canyon boundary. (As discussed below, a similar 'preference' angle of about 30° is reported by Dakoulas & Hashmi[34] for an earth dam in a rectangular canyon, subjected to incident *SH* waves.)

In the case of Type 2 valley, it is easier to identify the generation of Love waves by observing the natural frequencies and the response cutoff for frequencies below the fundamental Love-wave natural frequencies. For both Type 1 and Type 2 valleys, more dispersion lobes are observed when the layer is shallower. (Note that the phase velocity varies in Type 1, but it remains fairly constant for the lobes in Type 2 due to the practically constant thickness of the layer.) On the other hand, deep valleys tend to show higher response at their center and less response near the edges compared to the response of shallow valleys.

Bard & Bouchon[15] report that a comparison between the responses of the two valley geometries shows that, for the same depth over width ratio, the Love wave amplitude is much higher in Type 1 than in Type 2. This is because in Type 1 valley, as waves propagate from the edges to the center, the continuous increase of depth reinforces the Love waves and the center experiences the maximum response. Qualitatively similar response characteristics are expected in the case of an earth dam in the Type 1 valley, subjected to a ground excitation. It appears that the concentration of large amplitude response at the surface of the valley (and similarly at the crest of a dam) may be due to both a combination of the interference of Love waves and of wave focusing effects. These effects of the Love waves have been clearly demonstrated in the aforementioned studies. The wave focusing effect, reported by Trifunac[162] and Wong & Trifunac,[170] should not be perceived as only a different way of interpreting the effect of Love waves; the development of wave focusing in a dam on rigid canyon (e.g. Dakoulas & Gazetas[32]) suggests that these two are different phenomena.

Finally, regarding the Type 2 layer, in which the canyon effects are less important, its response is closer to the response of a flat layer, with the only exception the presence of Love waves propagating along two opposite directions.

4.3 3D response to dams to inclined plane *SH* waves

It is reasonable to expect that qualitatively similar wave phenomena occur in alluvial valleys and in dams, when the underlying canyons are of the same shape (see for instance the work of Nahhas,[109] who makes use of this similarity). On the other hand, the geometry of a dam is always 3-dimensional, even if it is built in a canyon of prismatic (2-dimensional) shape, since additional reflections take place on the inclined faces. The study of this problem is still at an early stage.

In a first attempt to develop a simplified analytical solution to the problem, Dakoulas & Hashmi[34] derived a mathematical solution for the steady-state response of embankment dams in rectangular canyons, subjected to obliquely incident *SH* waves. The dam is idealized as a 2-dimensional *homogeneous* triangular shear wedge, consisting of a linearly hysteretic material (Fig. 6). The excitation consists of harmonic *SH* waves of a constant ampitude, U_1 and frequency, ω, traveling from the left to the right at an angle θ from the vertical. The lateral displacement, u_1, of the incident waves has the form

$$u_1 = U_1 e^{i\omega(t - x/V_x + z/V_z)} \tag{3}$$

in which V_x and V_z are the phase velocities along the x and z directions given by

$$V_x = \frac{V_{\text{canyon}}}{\sin\theta} \qquad V_z = \frac{V_{\text{canyon}}}{\cos\theta} \tag{4}$$

These waves impinge on the left vertical abutment and the base of the dam, but they leave the right vertical abutment in a shadow zone. Nevertheless, the right boundary is subjected to waves which propagate through the dam reflecting on and transmitting through it. Consequently, the total excitation along the base and the two vertical abutments varies from point to point in both amplitude and phase and is determined by considering the dam-canyon interaction. Figure 6(c) illustrates schematically the incidence, reflection and transmission of the *SH* waves on the dam canyon interface and the free surface. Some additional reflections along the surface of the halfspace in front of the canyon, caused by the waves $U_2(z)$ reflected on the left vertical boundary (Fig. 6(c)) are neglected. The response of the dam to this asynchronous excitation is assumed to be only in horizontal lateral shear deformation with the upstream/downstream displacements, u, uniformly distributed across the width of the dam. In other words, the dam is idealized as a 'shear beam', a model that has been shown to be adequate for dynamic lateral response analysis of dams.[58]

From the dynamic equilibrium of an infinitesimal soil element of the dam (Fig. 6) and the stress-strain relationships, the equation of motion becomes

$$G_{\text{dam}}\left(\frac{\partial^2 u_t}{\partial x^2} + \frac{1}{z}\frac{\partial u_t}{\partial z} + \frac{\partial^2 u_t}{\partial z^2}\right) = \rho_{\text{dam}}\ddot{u}_1 \tag{5}$$

where $u_t = u_t(x, z, t)$ is the lateral total displacement

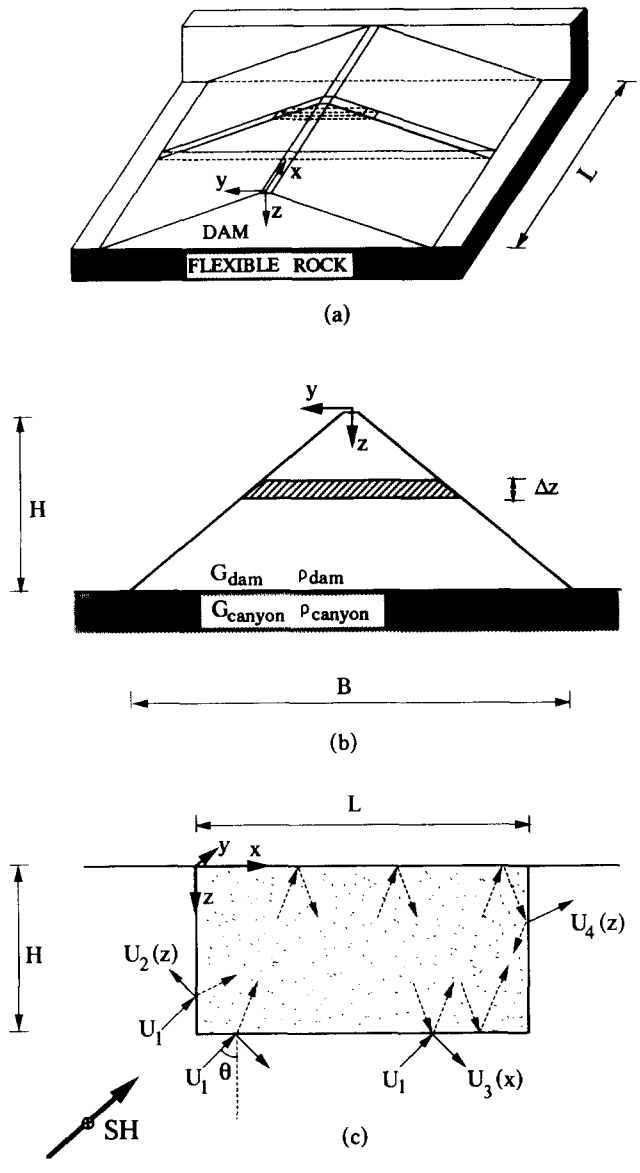

Fig. 6. Dam in Rectangular Canyon under Oblique-Wave Excitation (a) perspective view of the dam geometry; (b) dam cross-section; (c) longitudinal section illustrating incident, reflected and transmitted *SH* waves.

and $G^*_{\text{dam}} = G_{\text{dam}}(1 + 2i\beta_{\text{dam}})$, in which G_{dam} is the shear modulus and β_{dam} is the linear hysteretic damping of the dam; $i = \sqrt{(-1)}$. The solution to eqn (5) must satisfy the boundary conditions of zero shear stress τ_{yz} at the dam crest, of continuity of displacements along the dam base and the left and right vertical boundaries, and of continuity of shear stresses τ_{yz} at the dam base and τ_{yx} at the left and right vertical boundaries. The solution is derived by taking finite-cosine Fourier transform in the x direction and Hankel transform in the z direction while enforcing the boundary conditions. The amplification function, AF, for harmonic steady-state response, is computed with reference to the acceleration of the outcrop rock, the amplitude of which is twice the amplitude of the

incident wave. $AF = AF(x, z, \omega)$ is given by

$$AF = \left| \frac{U_t}{2U_1} \right| = \frac{1}{U_1} \left[\sum_{j=1}^{\infty} \left(\frac{\tilde{u}(0, \mu_j) J_0(\mu_j z/H)}{\pi J_1^2(\mu_j)} + \frac{2}{\pi} \sum_{1}^{\infty} \frac{\tilde{u}(n, \mu_j) J_0(\mu_j \eta) \cos(n x \pi / L)}{J_1^2(\mu_j)} \right) + U_b(x) \right] \quad (6)$$

in which U_t is the amplitude of the total motion, $U_b(x)$ is the amplitude of the motion at the base, $\tilde{u}(n, \mu_j)$ is the transformed solution, $J_0(\ )$ amd $J_1(\ )$ are Bessel functions of first kind, μ_j are roots of $J_0(z) = 0$, H is the height, and L is the length of the dam. ($U_b(x)$ is computed by solving the system of equations expressing the boundary conditions.)

The method has been used in a parametric study to investigate the effects of: (a) the angle of incidence, (b) the velocity ratio, and (c) the canyon narrowness, on the amplification function (AF) of displacement or acceleration.

Effect of the angle of incidence

The results of the parametric study show that the angle of incidence, θ, has an appreciable effect on the largest amplitude and the spatial variation of amplification. In fact, the effect is more significant for the spatial variation rather than its maximum value. Figure 7 shows the midcrest amplification of a dam with length-over-height ratio $L/H = 3$, S-wave velocity ratio $V_{canyon}/V_{dam} = 3$, mass density ratio $\rho_{canyon}/\rho_{dam} = 1{\cdot}3$, and material damping ratios $\beta_{dam} = 0{\cdot}10$ and $\beta_{canyon} = 0$, for eight angles of incidence $\theta = 0°$, 5°, 10°, 20°, 30°, 45°, 60° and 75°. For the cases examined, the maximum response is obtained at an angle $\theta \approx 30°$–35° and is about 25% higher than the response caused by vertically propagating waves. This is in agreement with the findings for the response of an alluvial valley to obliquely incident SH waves by Bard & Bouchon,[15] who reported a 'preference' angle of about 30°. For the dam, this maximum may be explained by the fact the response depends on the interference of waves transmitted through the base and the vertical abutments: for $\theta = 0°$ the motion is synchronous at the base, but asynchronous at the vertical abutments; as θ increases, however, the motion becomes more asynchronous at the base and less asynchronous at the left vertical boundary, resulting in a maximum response at $\theta \approx 30°$–35°. Moreover, as θ increases, a gradual shift of the location of the peak response is observed from the mid-crest (corresponding to $\theta = 0°$) to the right side of the dam. With increasing θ, waves traveling from left to right along the dam reflect mostly on the right side of the dam crest and part of them returns to the canyon, while the rest of them continue with a series of reflections on the dam boundaries (see Fig. 6(c)). The constructive interference of these waves produces an increased response at the right side of the crest. This can be seen in Fig. 8 which illustrates the spatial variation of amplification along the

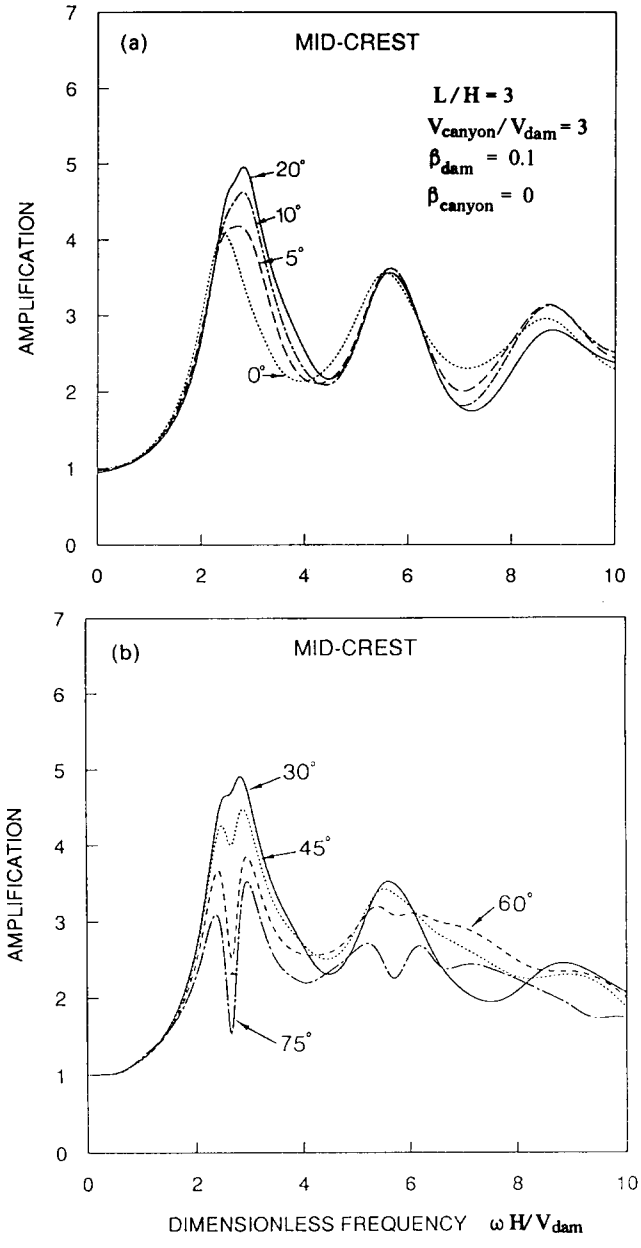

Fig. 7. Mid-crest amplification versus dimensionless frequency for a dam in rectangular canyon subjected to SH waves incident at θ equal to: (a) 0°, 5°, 10°, and 20° and (b) 30°, 45°, 60° and 70°.

crest of the dam for waves striking at $\theta = 30°$, at several wavelength-over-dam length ratios, λ/L. Evidently, the shaking is most violent *not* at midcrest but at locations closer to the abutments. Additional results show that the angle of incidence θ affects also significantly the variation in amplitude and phase of the total motion along the base and the two abutments of the dam.

For incident waves with large wavelength λ (e.g. $\lambda \geq 4L$), the dam appears as a small 'detail' in the halfspace and is practically ignored by the propagating waves. Hence the dam-canyon system tends to vibrate like a halfspace excited by SH waves, showing little variation of response along the crest of the dam.

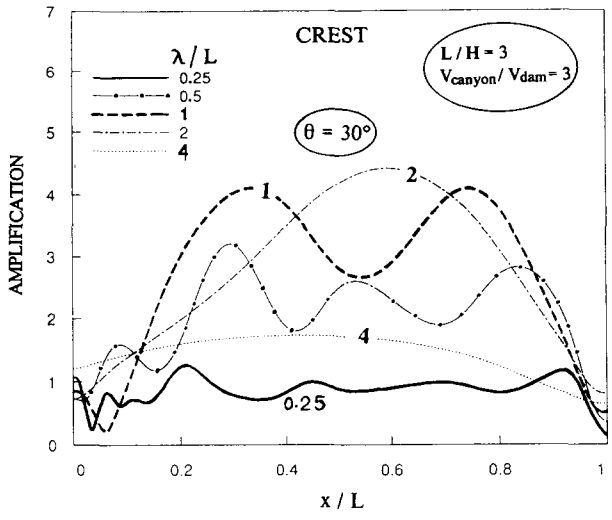

Fig. 8. Spatial variation of amplification along the crest of a dam in rectangular canyon subjected to oblique *SH* waves, for four values of the ratio of the wavelength to the canyon length *L*.

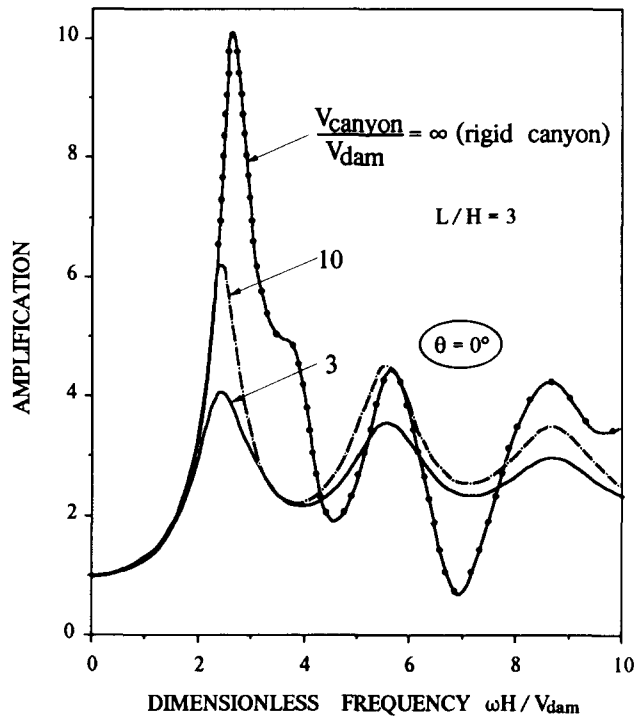

Fig. 9. Mid-crest amplification versus dimensionless frequency for three dams with *S* wave velocity ratios V_{canyon}/V_{dam} = 3, 10 and ∞ (rigid canyon) in rectangular canyons subjected to vertically propagating *SH* waves.

These results are in qualitative agreement with Trifunac[161,162] who obtained the amplification of motion at the surface of an alluvial deposit in a semi-cylindrical valley subjected to obliquely incident *SH* waves. The maximum response of the dam is obtained at its fundamental natural frequency. With decreasing λ/L ratios ($\lambda/L < 2$) the high frequency motion at the dam-canyon boundaries excites high-frequency vertical and longitudinal modes of vibration, in addition to lateral, displaying a larger number of peaks along the dam crest. A very high-frequency input excitation (i.e. with $\lambda/L = 0{\cdot}25$), causes an overall de-amplification of the response at the crest due mainly to the very asynchronous motion along the dam-canyon boundaries (Fig. 8). On the other extreme, when $\lambda/L > 4$ the response decreases again, since large-wavelengths *SH* waves hardly 'feel' the irregularity caused by the presence of the dam.

Effect of the S-*wave velocity ratio* V_{canyon}/V_{dam}

Parametric results show that the flexibility of the canyon rock (abutments and base) has a dramatic effect on the response of the dam, as it affects the amount of reflected energy that is radiated back into the halfspace (canyon). The presence of a flexible canyon-rock tends to reduce the amplification peaks at resonance, particularly with weak seismic excitation during which there would be little degradation of soil stiffness. Figure 9 plots the amplification for a dam having $L/H = 3$, and three different *S*-wave velocity ratios $V_{canyon}/V_{dam} = 3$, 10, and ∞, subjected to vertically-propagating *SH* waves. Notice that the midcrest amplification is about 4 for $V_{canyon}/V_{dam} = 3$, about 6·2 for $V_{canyon}/V_{dam} = 10$, and about 10 for $V_{canyon}/V_{dam} = \infty$. This clearly demonstrates that the simple assumption of a rigid base may be conservative in rectangular canyons.

Effect of canyon narrowness

For a given canyon shape, the canyon narrowness maybe expressed through L/H. With both synchronous and asynchronous excitation as the canyon narrowness increases the lateral response of the dam for the high frequency vibrational modes tends to increase. This is translated into higher accelerations and perhaps smaller displacements and shear strains within the dam; accelerations may be affected by many more modes (at least 10) than the displacements and strains (not more than 3 or 4). However, for very long dams, high frequency asynchronous excitation results in no amplification ($AF \approx 1$) while synchronous excitation induces much higher amplification ($AF \approx 2$ to 5, for the studied examples). This is hardly surprising since for high frequency excitation the wave length λ is very small and, therefore, there is significant destructive interference of the wave transmitted through the very long base of the dam resulting into $AF \approx 1$. Also, for long dams subjected to asynchronous motion, standing waves at certain frequencies have a stationary node point at midcrest.

Nahhas[109] developed a Boundary Integral Equation (BIE) type algorithm to analyse several simplified 2D and 3D earth dam models subjected to incident *SH*, *SV* and *P* waves. While the main emphasis of his research was the development and verification of a numerical tool, the results of a limited number of 3D analyses indicate that the distribution of crest amplifications of dams subjected to *SH* waves are in qualitative accord with the findings

outlined in the preceding paragraphs. (However, consistent comparisons are not possible due to differences in the geometrical and material characteristics assumed for the dams). He concludes that the assumption of a rigid canyon eliminates important anti-symmetric modes of vibration, affecting the characteristics of the response. A comparison of response characteristics using 2D and 3D models shows substantially different resonant frequencies and different amplitudes at high frequencies for the two models.

Response of earth dams to P *and* SV *waves*

In their study of the response of sediment-filled valleys subjected to incident *P* and *SV* waves, Bard & Bouchon[16] concluded that the phenomena are qualitatively similar to those observed during incident *SH* waves. The difference is that the canyon interface causes Rayleigh waves which are generated at the two edges of the valley. As the Love waves generated by incident *SH* waves, such Rayleigh waves propagate laterally trapped within the canyon, and may result into displacements substantially higher than the incident *P* or *SV* motion. It is reasonable to assume that similar conclusions might be drawn for earth/rockfill dams subjected to *P* and *SV* waves. Indeed, in a very limited study using a BIE formulation Nahhas found the response characteristics to incident *P* and *SV* waves to be qualitatively similar to those from incident *SH* waves.

Conclusion

The substantial midcrest amplifications computed in Section 3 for dams in rigidly-oscillating narrow canyons may decrease appreciably when the canyon motion is asynchronous, e.g. due to impinging plane seismic waves. Where the *S*-wave velocity contrast between dam and canyon is small, midcrest accelerations may decrease by a factor of about 2, as significant amounts of wave energy radiate back into the canyon halfspace. All this, however, is for dams assumed to be homogeneous; if material inhomogeneity were realistically taken into account (a formidable task up to now), the 'whip-lash' effect would become stronger and midcrest amplification would tend to increase.[58] Thus, in practical situations, one has to judge the relative significance between the (beneficial) incoherence of ground excitation and the (detrimental) inhomogeneity of rockfill. It is plausible that, in some cases, the response of the dam would be close to the one predicted (with the methods of Section 3) under the assumptions of uniform stiffness and synchronous excitation — provided that nonlinearities are unimportant.

5 SEISMIC ANALYSIS AND DESIGN OF CONCRETE-FACED ROCKFILL (CFR) DAMS

5.1 Introduction: the CFR dam

The concrete-faced rockfill (CFR) dam has been used with increasing frequency in recent years, in many parts of the world. In addition to being a natural choice where suitable clayey core material is not available in the vicinity of the project, the CFR dam has in many cases been found to be the least-cost alternative dam design. As worldwide experience is accumulating on the long-term performance of CFR dams, their popularity will probably increase in coming years. Current design trends and construction/performance records of many recent dams can be found in the proceedings of a 1985 ASCE symposium[27] and an accompanying issue of the ASCE Journal of Geotechnical Engineering (Vol. 113, No. 10, October, 1987).

The basic features of the CFR dam are outlined herein with the help of Fig. 10, which shows a cross-section, a view of the upstream face, and some characteristic details of a typical design. In contrast with the earth-core rockfill (ECR) dam, the main body of the CFR dam consists exclusively of rockfill, all of which is located downstream from the water thrust; the latter acts externally on the upstream reinforced-concrete face and contributes to increasing the stiffness and stability of CFR dams. Hence, much steeper slopes (ranging from 1 : 1·3 to 1 : 1·6) are attainable in DFR dams.

Their success depends, in addition of course to material quality and degree of compaction of the rockfill, on the successful construction of the face slab, the toe slab ('plinth'), and the watertightness of their various joints. The perimetric toe slab ('plinth') is typically 4 m wide and is intended to provide a watertight connection between the concrete face and the dam foundation (along the valley and the abutments). It is shaped to provide an apron or cap for foundation grouting operation, and a surface in the plane of the face from which face-slab slip forming can start. If suitable foundation material is not found near the surface, a continuous trench is made along the plinth, to eliminate the possibility of erosion or piping in the foundation.

The face slab is usually made of 20 MPa-strength concrete, with 0·4% reinforcing in each direction placed in the center of the slab. Its thickness is variable along the height, starting at 0·30 m–0·40 m near the crest and increasing by approximately $0{\cdot}002\,h_w$, where h_w is the depth of water (in meters). Crucial is the design and construction of the perimetric joint between face slab and plinth, as this joint always opens up and distorts moderately when the reservoir is filled. A double (and sometimes triple) line of defence is provided against this potential source of leakage (see Fig. 10): surface-mastic securely covered with a PVC band at the top; a copper waterstop underlain by a zone of sand-asphalt mixture at the bottom; and perhaps a PVC waterstop at the middle of the face slab.

Face slabs are placed in vertical strips, typically 15 m wide, by slip form continuously from bottom to top, where they culminate in an *L*-shaped 3–5 m high cantilever crest wall, the cost of which is more than offset by

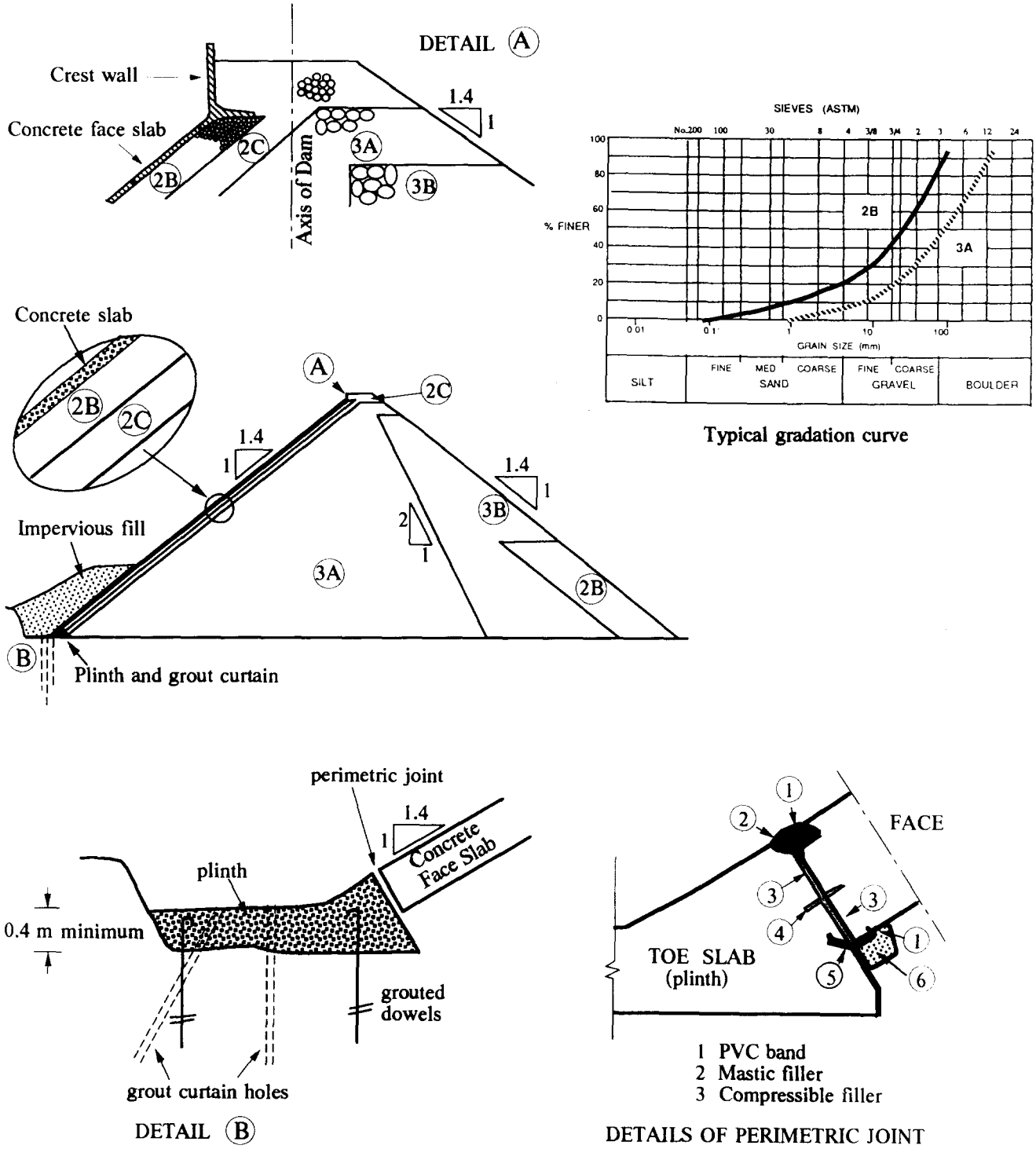

Fig. 10. Typical cross-section, details, and material composition of a CFR dam.

saving a slice of downstream rockfill.[49] This type of crest wall, introduced and developed in Australia (since Makintosh dam, 1981), is currently adopted in most dams built in seismically inactive areas.

The upstream zone supporting the face slab consists of smaller-size rock than the main body of the dam to facilitate slope trimming and compaction and thus minimize differential slab movements. Another role of this zone is to be of somewhat low permeability so as to limit leakage into the dam to that which could safely be passed through the downstream zones, should the cofferdam be overtopped before the concrete face slab is constructed. A disagreement exists among experts over a third possible role of this zone: to limit the leakage due to cracks in the concrete slab or from defective/damaged waterstops. Sherard[155] has argued that this zone should

consist of crushed-rock or alluvial sandy-gravel with an average of about 40% of particles passing the No. 4 sieve (i.e., finer than about 5 mm), to limit its permeability coefficient to less than 10^{-3} cm/s. Others, however,[23] have pointed to some undesirable effects of such material composition, including the slightly lower shear strength and the likelihood that this zone may become and remain saturated — with potentially detrimental effects during strong seismic shaking.

Compaction of the rockfill to achieve a high density is a requirement to minimize deformations and face-slab distress and leakage. One of the factors controlling the compression modulus of rockfill is its gradation. Well graded materials, with smaller-size particles filling the voids between larger rocks, yet maintaining free-draining characteristics, have led to very satisfactory design. High moduli of deformation have in fact been achieved in CFR dams with rockfill having uniformity coefficient of 20 or higher and containing about 30% of material smaller than 1″. Measurements have also shown that rockfill is about 3 times as stiff in the horizontal direction than in the vertical.

5.2 Review of studies on seismic response of CFR dams

The anticipated response and performance of modern CFR dams under strong earthquake excitation has received only limited attention in the published literature.[21,63,65,125,154] Many engineers have argued that the CFR dam is inherently safe against potential seismic damage[154] since: (i) the entire CFR embankment is dry and hence earthquake shaking cannot cause porewater pressure buildup and strength degradation; and (ii) the reservoir water pressure acts externally on the upstream fact and hence the entire rockfill mass acts to provide stability, whereas by contrast in ECR dams this is true only for the downstream rockfill shell.

Notwithstanding the merit of these arguments, it is pointed out that to date no CFR dam has been tested under strong seismic shaking to prove the adequacy of its various design features. In fact most CFR dams have been built in areas of very low seismicity, such as Australia and Brazil, and it seems that some of the design concepts and features have evolved with no consideration of their seismic performance, as we have hinted in 5.1.

Seed *et al.*[152] reported a comprehensive set of conventional analyses aimed at estimating the magnitude of sliding deformations of typical CFR dams subjected to base accelerations with a peak of 0·50 g originating at sources of magnitude ranging from M $\approx 6\frac{1}{2}$ to M $\approx 8\frac{1}{4}$. To this end, analyses were performed in two stages, accepting the well-established *decoupling* of the dynamic response analysis from the sliding deformation analysis.[86] In the first stage, equivalent-linear plane-strain analyses were conducted, appropriated for tall dams built in very wide valleys. With rockfill shear modulus dependent on both static mean confining stress (σ_0') and cyclic shear-strain amplitude (γ), two idealized 500 ft-high (≈ 150 m) cross-sections were analyzed: Section No. 1 having a crest width of 40 ft (≈ 12 m) and side slopes, both up- and down-stream, of 1 : 1·6; and Section No. 2 with the same crest width of 40 ft but side slopes, both up- and down-stream, 1 : 1·5 for the lower $\frac{3}{4}$ and 1 1·8 for the upper $\frac{1}{4}$ of the dam. The computed peak values of response accelerations to a 0·50 g artificial base accelerogram are portrayed for the two sections in Fig. 11 and reveal that near-crest accelerations slightly exceed g.

In the second stage permanent deformations were computed using the Seed–Makdisi version of the Newmark[111] 'sliding-block' analysis. The method requires the computation, for a number of potentially sliding wedges, of the (spatially) average 'driving' acceleration history, $k_a(t)$, expressed conveniently by its peak value K_a, and of the 'critical' (yield) acceleration, k_y, beyond which sliding deformation begins. Assuming an angle of shearing resistance at low confining pressures equal to 54°, Seed *et al.*[152] found that 'the computed deformations for the downstream slope are less than 1 ft . . . provided the magnitude of the earthquake is $7\frac{1}{2}$ or less. However, when the magnitude is about $8\frac{1}{4}$ deformations as large as 7 ft may possibly occur in the downstream direction. Such deformations are undesirably high and would indicate the need for flatter slopes in order to limit the movements to acceptable values.' (cit.)

Finally, utilizing the results of a study with peak base acceleration and earthquake magnitude as the parameters, Seed *et al.* make the recommendations given in Table 3 for the Downstream (DS) slopes that are deemed necessary to limit sliding deformations to 1 ft or 2 ft. Apparently, the recommended slopes are appreciably flatter than the slopes currently used in design; in areas of high and very high seismicity the recommended values are of the order of 1.6 or greater.

Seed *et al.*[152] also called attention to some limitations of their analyses. For example, the key assumption in the sliding-block analysis that permanent deformation takes place on individual planes is only a crude approximation: actual deformations are likely to be spread out over a zone, leading to bulging rather than planar sliding. In addition, other forms of instability are plausible such as progressive rolling of large stones on the down-stream face.

It is further noted that this study did not address: (i) the potential effects of dam shaking on the concrete face slab and on the crest wall, and (ii) the important influence of a 3D narrow canyon geometry on the intensity and frequency composition of dam shaking. Therefore, we believe that the conclusions of their study (summarized in Table 3) may turn out to be not as conservative as initially thought of by some engineers.[154]

The study of Bureau *et al.*[21] has included discussions on the seismic performance of rockfill dams, in general, and on the possible modes of failure of CFR dams. An empirical chart has been presented relating observed

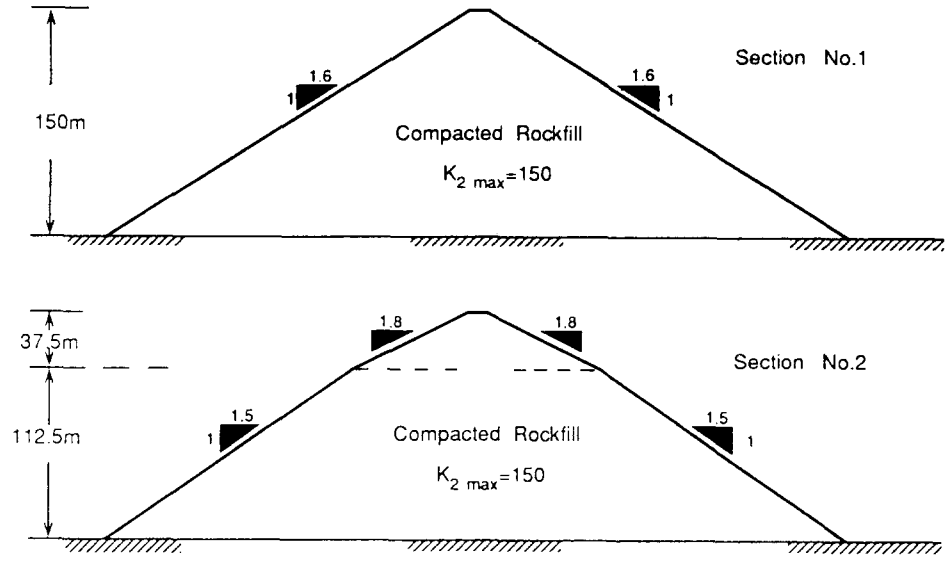

Cross-sections of dams used for analysis

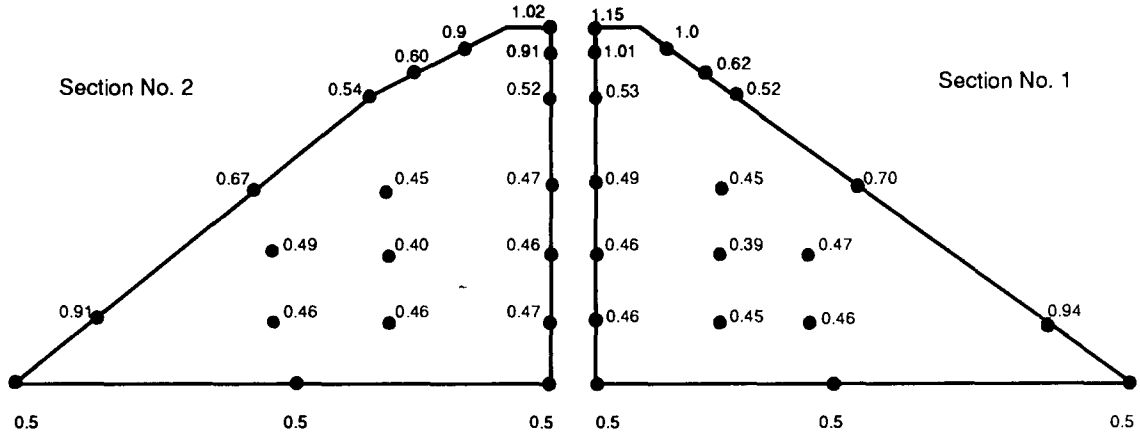

Fig. 11. Peak accelerations (in g) developed in plane dam sections Nos. 1 & 2 for earthquake producing 0·5 g at base (from Seed *et al.*[152]).

Table 3. Slopes recommended by Seed *et al.*[152] for CFR dams in seismic areas

Earthquake Magnitude	Peak Crest Acceleration	Average DS Slope for Displacements of 2 ft or more	Average DS Slope for Displacements of 1 ft or less	Seismicity of the Area
6·5	$<0{\cdot}25$ g	1·35	1·4	
6·5	$\approx 0{\cdot}45$ g	1·4	1·4	Low
7·5	$\approx 0{\cdot}45$ g	1·4	1·4	to
8·5	$\approx 0{\cdot}45$ g	1·45	1·45	Moderate
6·5	$\approx 0{\cdot}75$ g	1·5	1·5	
7·5	$\approx 0{\cdot}75$ g	1·55	1·6	
8·5	$\approx 0{\cdot}75$ g	1·65	1·7	High
6·5	$\approx 1{\cdot}0$ g	1·55	1·55	
7·5	$\approx 1{\cdot}0$ g	1·6	1·65	Very
8·5	$>1{\cdot}0$ g	1·8	1·8	High

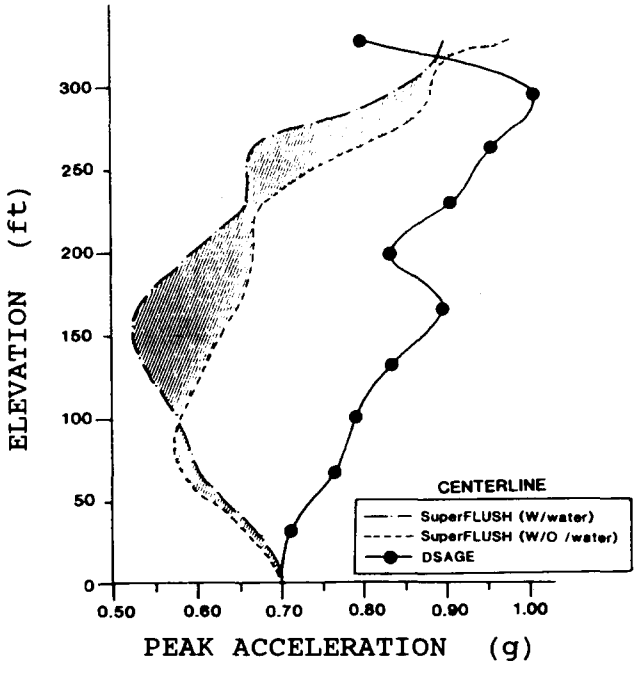

Fig. 12. Comparison of the distribution along the centerline of the peak accelerations computed with various nonlinear codes, for a hypothetical CFR dam model. (From Bureau *et al.*[21])

earthquake-induced crest settlements to the index ESI = $A(M - 4{\cdot}5)^3$, named 'Earthquake Severity Index,' where A = the peak ground acceleration divided by g, and M = the earthquake magnitude. Moreover, their paper has outlined a numerical formulation ('Dsage') for computing the nonlinear response of CFR dams and evaluating the complete distribution pattern of permanent deformations, without a need to use the (simplified) Newmark procedure. An elastic-perfectly-plastic constitutive law based on Coulomb's failure criterion with pressure-dependent friction angle was implemented into an explicit finite-difference scheme and analyses were performed in the time domain. To avoid unrealistic tension in the rockfill, a tension-cutoff formulation was included allowing for the generation of a 'crack' whenever the minor principal stress became negative.

In addition to 'Dsage', Bureau *et al.*[21] utilized an equivalent-linear finite-element formulation, 'super-flush', to study the effect of fluid-dam interaction and to estimate the seismic axial-forces and bending-moments on the concrete-face slab. For a hypothetical 100 m-high dam subjected to an artificial accelerogram (pga = 0·70 g, strong-motion duration $\approx$ 13 s), the peak acceleration at various depths computed with the two codes differ somewhat, as seen in Fig. 12. This is not surprising: with such a high intensity shaking, equivalent linearization would certainly be a crude approximation. On the other hand, one must keep in mind that even the nonlinear constitutive model used in 'Dsage' may not represent rockfill behavior adequately. For instance, perfectly plastic rather than strain-hardening behavior is assumed; this may impose a spurious upper limit on the largest peak acceleration that can be 'transmitted' to the crest of the dam. And of course, the variation of secant modulus versus strain from this elastoplactic model can not possibly coincide with the experimental $G - G(\gamma)$ curve incorporated in the equivalent-linear formulation.

Important conclusions of the Bureau *et al.*[21] study are: (1) Hydrodynamic effects can be safely ignored in estimating the seismic response of CFR dams, but the static water pressure from the reservoir contributes to increasing the lateral deformations in the downstream direction, when plastic straining occurs. (2) Most of the dam section under strong (pga $\approx$ 0·70 g) excitation is in a state of plastic deformation; thus, distributed slumping rather than failure along a discrete surface takes place. (3) Permanent deformations seem to concentrate in the upper third of the dam, a result also confirmed by observations on El Infiernillo Dam.[135] (4) Crest deformations of the order of 1 m remain following this strong shaking; and in general, it is concluded that crest settlements of modern CFR dams would not exceed 1% or 2% of the dam height under the most severe earthquake shaking. According to Sherard & Cooke[154] this would be an acceptable performance since 'a sudden crest settlement of 0·01 H will not threaten the safety of a modern CFRD'.

A qualitative picture of the modes of seismic failure of CFR dams might be obtained through Shaking-Table tests of small-scale physical models. Such a study was reported by Han *et al.*,[65] who used a 1·0 m-high model having up- and down-stream slopes of 1 : 1·4, a 4 mm-thick face slab consisting mainly of gypsum and having a tensile strength of up to 300 kPa, a 2·5 cm thick supporting zone of sand with mass density of 1.7 Mg/m^3, and a main body consisting of sand-and-gravel compacted to a 1·6 Mg/m^3 density. Base accelerations reached 0.60 g and permanent deformations started at 0.14 g. They observed that, initially, sliding was confined to shallow wedges in the vicinity of the crest. With increasing acceleration amplitudes the size of the sliding zone increased and rolling/sliding of gravels occurred primarily downstream. At even greater amplitudes the face slabs lost support, deformed as a cantilever, and ruptured in violent vibration.

The above observations support the concept of sliding mode of deformation predicted in the theoretical studies. However, in view of the inadequacy of such small-scale models to reproduce the significant effects of gravity on material behavior, the results of this study should be interpreted with caution, and only qualitatively. It would be of great interest to attempt realistic modeling of CFR dams in a large centrifuge; the authors are not aware of any such study up to now.

Finally, it is worth mentioning the published seismic analysis of the (then under construction) Balsam Medow Dam (38 m) in California. Using the conventional seismic-response-sliding-deformation procedure they found that

a 'broad-band' 0·15 g ground accelerogram used as excitation produces peak crest accelerations of about 0·65 g — a substantial amplification of nearly 4·5. Nevertheless, and despite the steep slopes of 1 : 1·3, they unexpectedly report practically zero computed permanent deformations. Perhaps what they refer to is displacements over long sliding wedges extending throughout the height of the dam. On the other hand, for shallow sliding wedges extending 10 m–20 m below the crest the critical 'yield' acceleration k_y is 47° of the order of 0·18 g for $\phi = 47°$, compared with peak 'driving' acceleration K_a exceeding 0·60 g; this might lead to permanent displacements of the order of 0·50 m.

5.3 A case study: CFR dam in narrow canyon — potential problems and suggestion solution

All the aforementioned studies are based on 2D analyses of the seismic response that assume plane-strain conditions. This is exactly valid only for infinitely-long dams subjected to a 'synchronous' base excitation. Many CFR dams, however, have been and are being built in narrow valleys consisting of good quality rock, as evidence in the proceedings of the 1985 Symposium.[27] As already discussed in Section 3, the presence of rigid abutments creates a 3D stiffening effect, whereby natural periods decrease and near-crest accelerations increase sharply as the canyon becomes narrower. The potential consequences of such canyon effects for the performance of CFR dams against strong shaking are explored herein with the help of a case study involving state-of-the-art analyses of an actual design of a 135-high CFR dam (hereafter to be called 'M' Dam) presently under construction in an area of relatively high seismicity.

5.3.1 Geometry and material modeling; method of seismic response analysis of the 'M' CFR dam

The original design of the Dam, that is studied herein, following the previously (Section 5.1) outlined established practice, called for 1 : 1·4 up- and down-stream slopes, a 4 m-high crest retaining ('parapet') wall, crest width of 5 m, and a face slab without expansion joints and hence no waterstops for either the horizontal or the vertical construction joints.

As portrayed in Fig. 13, the geometry of the 'M' canyon can be approximated with sufficient accuracy as a semi-cylinder, of radius R equal to the height H of the maximum dam cross-section:

$$R = H = 135\,\text{m} \tag{7}$$

(Note that approximating the canyon as a triangular prism with a maximum height H and each abutment at an angle of about 40° to the horizontal, might have also been acceptable. However, as it has been shown by Makdisi *et al.*,[90] and Gazetas,[59] these two geometries lead to quite similar results.)

The dynamic behavior of a rockfill 'element' is described through the small-strain shear modulus, G_{max}; the Poisson's ratio, ν; and the decrease of the secant shear modulus, G, and increase of the equivalent hysteretic damping ratio, β, with increasing amplitude of shear strain, γ. Since no experimental results had been available in this case, we resorted to the published empirical correlation:

$$G_{max} = 1000 \cdot K_{2,max} \cdot (\sigma_o)^{1/2} \tag{8}$$

where G_{max} and σ_o in units of lbs/ft^2 (1 lb/ft^2 $\approx$ 1/20 kPa). The value of $K_{2,max}$ for compacted gravels and rockfill appears to be in the range of 150–250. Back analysis of the response of Oroville Dam (California) to a weak seismic shaking gave $K_{2,max} \approx 170$.[101] This value was used as the best estimate in our dynamic response analyses. Of course, $K_{2,max}$ was also varied parametrically between 150 and 200, if only to confirm that the conclusions regarding the performance of the dam are not sensitive to the exact value of this parameter.

- Poisson's ratio ν for dry or nearly dry rockfill is taken equal to 0·25. Note that ν has only a marginal influence on the lateral oscillation, but may play a substantial role in longitudinal and especially vertical oscillations.
- Recent data is available for estimating the decline of G with increasing γ;[152] they reveal a faster rate of decay than the one measured for sandy soils and which was used in previous studies (by 'extrapolation'). Figure 14 plots the ratio G/G_{max} versus γ for rockfill, as used in this study.
- The data for estimating the growth of β with increasing γ show a slightly faster rate of growth than the one measured in sands and clays. The utilized β versus γ curve is plotted in Fig. 14.

Having modeled in a fairly rational way both geometry and dynamic properties of the 'M' Dam, seismic response analyses are performed using state-of-the-art methods. Specifically, in all cases, 'equivalent linear' viscoelastic analyses are performed, in which the shear modulus and damping ratio are obtained from Fig. 14 in conjunction with the 'effective' shear strain level of the previous iteration. The 'effective' shear strain is obtained as the $\frac{2}{3}$ fraction of the peak shear strain.

The aforementioned analytical solution of Dakoulas & Gazetas[32] for natural frequencies, mode shapes, and mode participation factors is utilized. Thus, for each linear analysis, model superposition in the time domain is performed, involving step-by-step integration of each of the 10 uncoupled differential equations of motion which correspond to the first 10 natural modes of oscillation of the 3D dam.

All three directions of seismic oscillation are considered: (i) lateral oscillation in the upstream-downstream direction; (ii) longitudinal oscillation in the direction of the crest axis; and (iii) vertical oscillation.

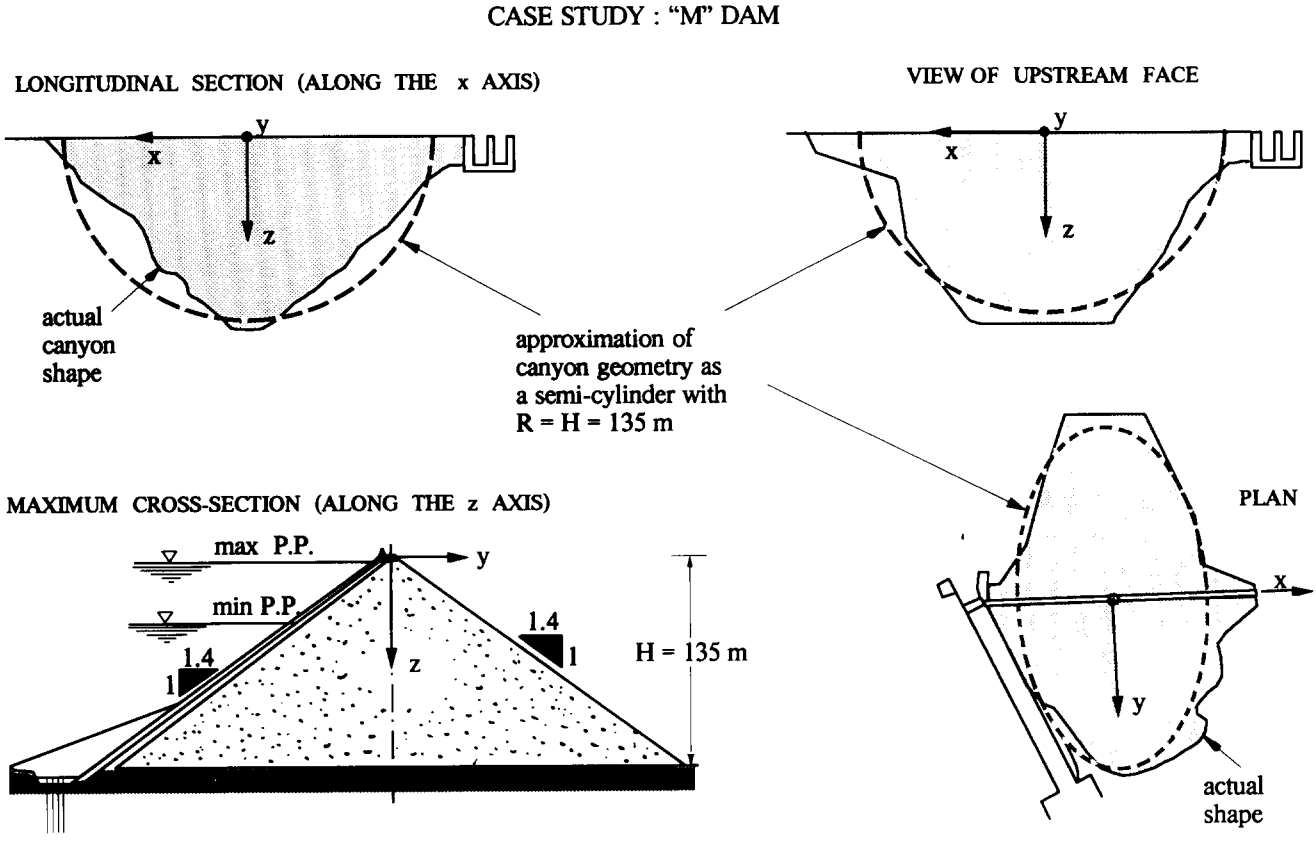

Fig. 13. Case study of a CFR dam: 'M' dam geometry and its idealization for dynamic response analysis.

However, results are discussed in detail for lateral oscillations and only the main conclusions are reported from the response in the other two directions.

5.3.2 Seismic hazard analysis and design ground excitations

A comprehensive study was performed to establish (a) the characteristics of the Design Earthquake and (b) several acceleration histories to be used as Design Ground Excitations. The first of these goals was achieved through a comprehensive investigation of the geologic and seismotectonic environment of the site, and a study of the seismic history and seismicity of the area. It was concluded that the Design Earthquake should be an event with the following characteristics:

- moment magnitude $M_w = 6{\cdot}5$ occurring at a normal fault, about 10 kilometers deep
- distance r_o of the dam site from the fault up to 10 kilometers (i.e., corresponding epicentral distance up to 15 km).

Some additional source parameters, such as the Seismic Moment $M_o = 2{\cdot}3 \times 10^{26}$ dyne-cm, the Brune Stress Drop $\Delta\sigma = 131$ bars, and the Corner Frequency $f_c = 0{\cdot}13$ Hz, were estimated from values reported in the literature for similar magnitude normal-fault events. Another characteristic frequency, f_{max}, needed for the description of the source was varied parametrically from 5 Hz to 20 Hz.

Following the current state-of-the-art, three different but complementary procedures are applied to arrive at realistic descriptions of the free-field ground motions at the dam site:

- numerical modeling of the earthquake source and the wave propagation to the site, that produces synthetic accelerograms

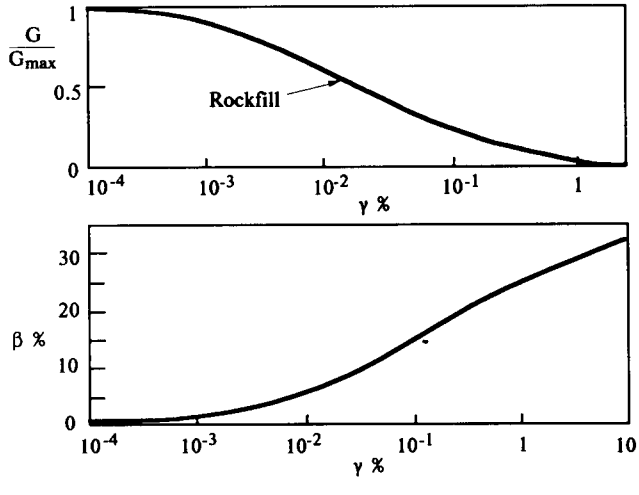

Fig. 14. Shear modulus reduction and damping ratio versus cyclic shear strain used for "M" dam rockfill.

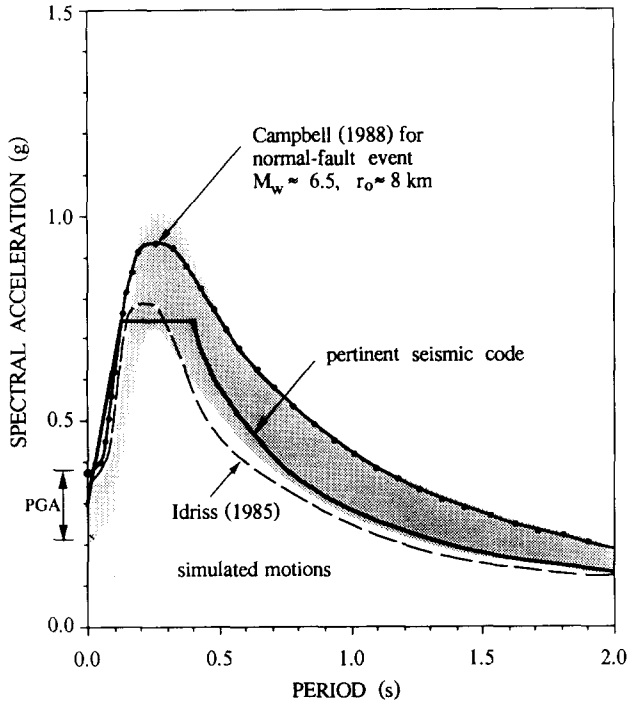

Fig. 15. Design response spectra derived with several procedures.

- empirical correlations (attentuation relations) between magnitude, M, source distance, r_o, and spectral accelerations, $S_a(T)$, for a number of periods T and 5% damping. Product: design response spectrum. Also incorporated: spectra given in relevant codes
- historic accelerograms recorded under conditions similar to those of the Design Earthquake (M, r_o, source mechanism, etc).

The results of the study are summarized in Fig. 15 in the form of design response spectra. It is noted that the various predictions for the peak ground acceleration (pga) range between 0·25 g–0·50 g, with an average of about 0·35 g. The acceleration spectral shapes show fundamental periods between 0·10 s and 0·40 s — as expected for free field motions on stiff and rock-like soil originating from an $M = 6{\cdot}5$ event. The largest values of S_a in this dominant-period range vary from about 0·70 g to 1.50 g.

5.3.3 Results: lateral seismic response

Figure 16 summarizes the results of the parametric dynamic response analyses in the form of distribution of peak absolute accelerations with depth, along the vertical axis z of the Dam. It is evident that the top third of the Dam (the near-crest region) experiences extremely strong shaking; crest accelerations in particular average about 1·50 g, with the smallest being about 1·15 g. This implies a crest-to-base amplification factor AF $\approx$ 5.

Smooth average distributions of peak accelerations

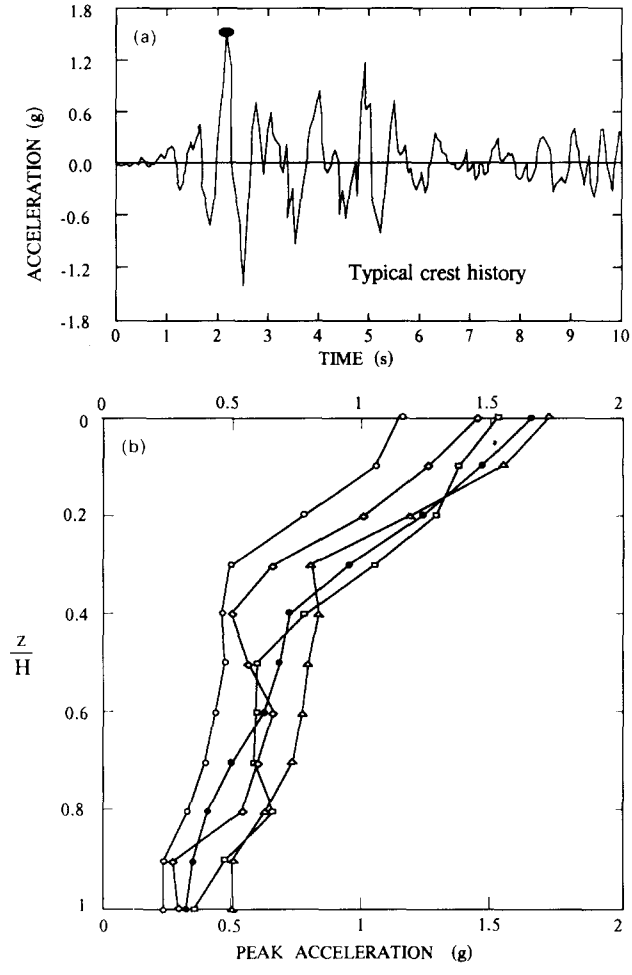

Fig. 16. 'M' dam: (a) typical computed mid-crest accelerogram (b) computed distribution of peak acceleration along the vertical z axis.

along the vertical (z) and horizontal axes of the Dam are depicted in Fig. 17. These distributions are utilized in the sequel when exploring the consequences of the Dam oscillation. From the corresponding smooth average distributions of peak shear strains along the vertical (z) axis it appears that shear strains do not exceed the moderate 10^{-3} (or 0·1%), despite the very strong shaking of the dam.

5.3.4 Evidence of realism of the results — peculiarity of CFR dams

As will be explained in the sequel, the consequences of the very high accelerations near the mid-crest of the Dam are likely to be very serious — not so much for the overall safety of the dam, as for the operation of the facility during its design life.

The question may be raised: Are such high response accelerations realistic? Or are they merely an artifact of the unavoidably simplified theoretical modeling? What evidence is there? . . .

Of course, the only unambiguous evidence (a 'proof') would come from an actually recorded response of a

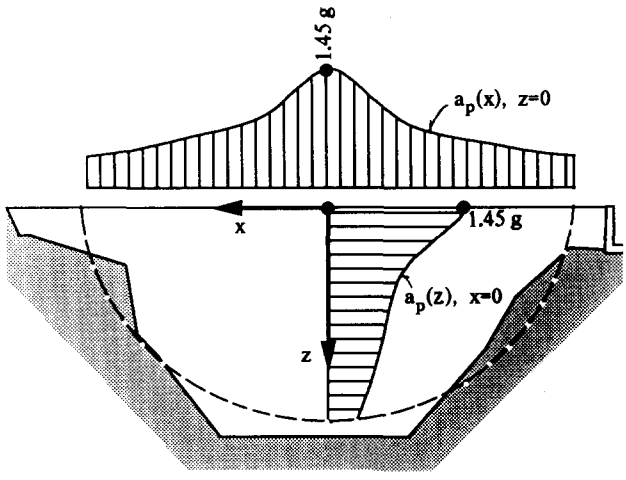

Fig. 17. 'M' dam: distribution of peak lateral accelerations along the crest and along the vertical z axis (average of all analyses.

similar (in height and canyon geometry) CFR Dam to a similarly strong shaking (pga $\approx$ 0·35 g) originating from an $M \approx 6{\cdot}5$ and $r \approx$ (5–10) km event. Unfortunately, no CFR dam has to date been subjected to even moderate (let along strong) ground shaking. Thus, the evidence presented herein serves only as an indirect corroboration. . .

There are two basic arguments in support of our findings: the first is based on theoretical results published by other researchers in this field; the second derives from field records of the seismic response of standard rockfill dams to weak ground motions. Specifically:

(a) Similarly high amplification of peak accelerations from the base to the crest in a narrow canyon have also confirmed by Seed and his coworkers at Berkeley. Using a 3D finite-element formulation,[90,101,152] they analyzed a dam with mild face slopes of 1 : 2 in a triangular-canyon with $L/H = 3$. As sketched in Fig. 18, an excitation with a pga = 0·20 g results in peak crest acceleration of about 1 g, corresponding to an amplification factor

$$AF = \frac{a_{p,\text{crest}}}{\text{pga}} \approx 5 \tag{9}$$

Moreover, because of the narrowness of the canyon, the peak crest acceleration is nearly two times the value predicted for an ∞-long dam, i.e. under 2D plane-strain conditions:

$$\frac{a_{p,\text{crest}}(3D)}{a_{p,\text{crest}}(2D)} \approx 2 \tag{10}$$

Performing 2-D plane-strain analyses for a CFR dam section Seed *et al.*[152] have found that a 0·30 g peak base acceleration from a $M = 6{\cdot}5$ earthquake leads to crest accelerations of 0·75 g. If the same dam is to be built in a canyon as narrow as in this case, the anticipated crest acceleration would be

$$a_{p,\text{crest}} \gtrsim 2 \times 0{\cdot}75\,\text{g} = 1{\cdot}50\,\text{g} \tag{11}$$

in full accord with our analyses.

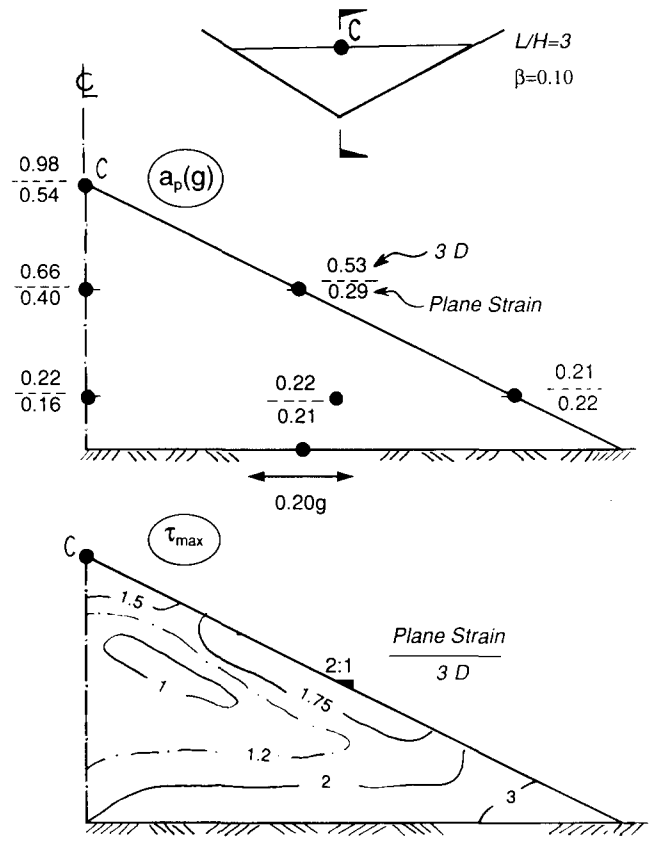

Fig. 18. Three-dimensional (3D) versus two-dimensional (2D) plane-strain analysis for a dam in a triangular canyon. Peak acceleration at the crest is under-predicted by the 2D analysis by a factor of 2. (From Makdisi *et al.*[90])

(b) Fortunately, there also exists a piece of field evidence suggesting that the predicted 3-D crest amplifications are realistic. It refers to the Kisenyama dam, in Japan, a 95 m clayey-core rockfill dam, built in 1969, sketched in Fig. 19. The dam is located in a narrow valley and founded on rock (slate). The similarity of its geometry with 'M' dam can hardly be overstated. On September 1969, shortly after completion, the dam was subjected to seismic shaking which produced the shown acceleration records at 5 seismometers installed in the dam (S_1, S_2, S_3, S_4) and at the downstream rock outcrop (S_5).

The substantial amplification by a factor of about 12 of the acceleration at the crest, and the resulting sharp attentuation of acceleration peaks with depth, are reminiscent of the distributions of peak accelerations portrayed in Fig. 17.

Since these motions were too small for this modern rockfill dam ($V_{s,\max} \approx 360$ m/s) to develop any noticeable nonlinearities, it may be concluded that, in addition to the small damping ratio (at most 2 to 3%), it is the narrow canyon and, to a lesser degree, soil inhomogeneity which have caused the relatively high accelerations at the crest of the dam.

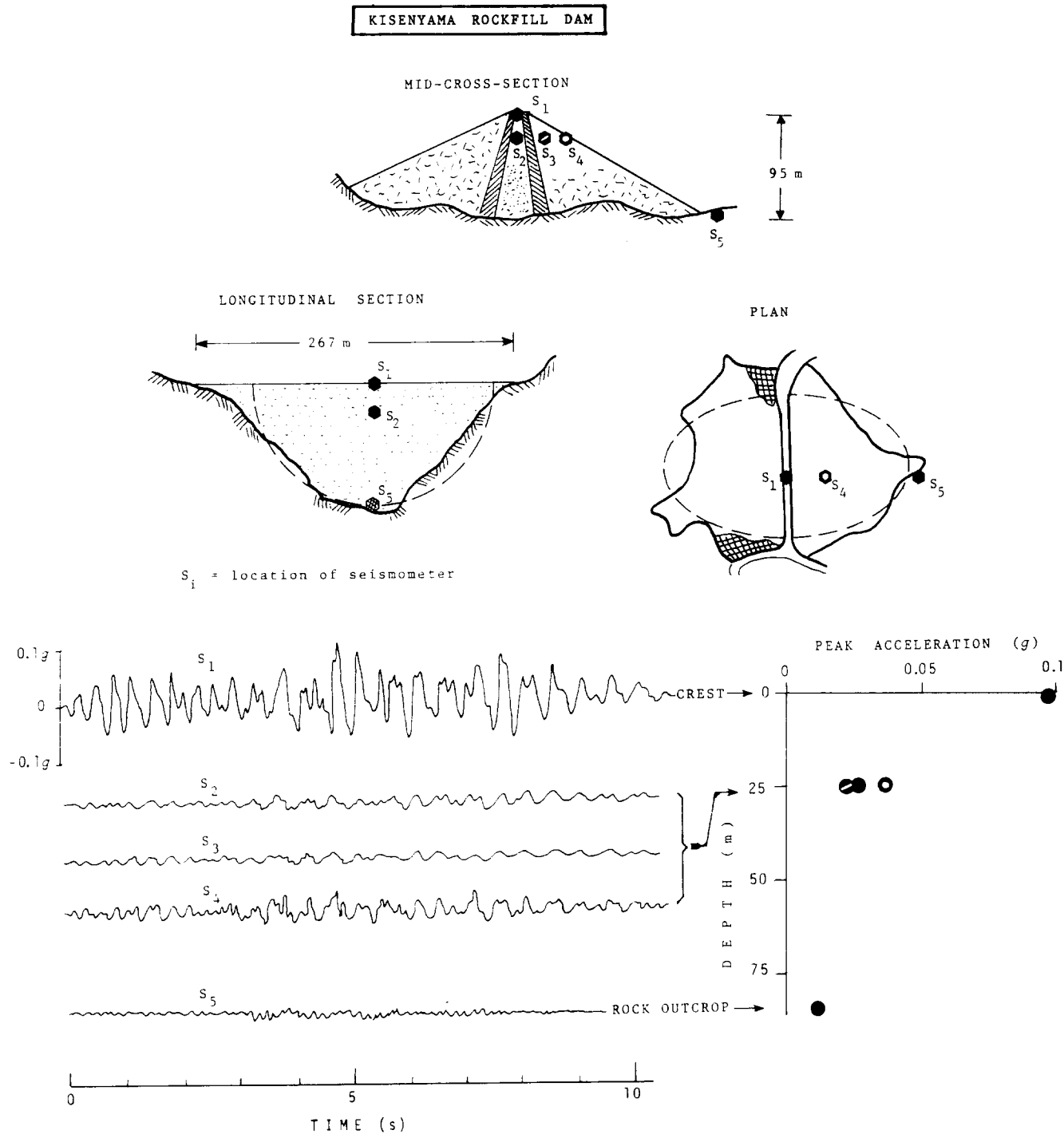

Fig. 19. Evidence of high mid-crest amplification of the peak accelerations in tall rockfill dams built in narrow canyons and subjected to weak seismic excitation: the case of Kisenyama rockfill dam in Japan.

During a much stronger excitation, however, Kisenyama would experience significant nonlinearities in the relatively soft clayey core. Such nonlinearities are doubly beneficial: they produce higher amounts of damping, and they tend to elongate the fundamental dam period, T_1, which might thus fall well outside the significant period range of the ground motion. Consequently the amplification base to crest would be reduced; values of $AF \approx 3$ have been obtained from records of El Infiernillo Dam in Mexico. A detailed account of this beneficial role of strong nonlinearities can be found in Ref. 58.

But, unfortunately, modern CFR dams do not contain the large 'flexible' mass of a clayey core. Moreover, they do not suffer from hydrostatic pore-water pressures which in other types of dams tend to reduce the effective overburden stresses in part of the dam. Instead, the water

pressures act externally and further increase the confining stresses in about half the dam section. All this makes such dams much stiffer and stronger than comparable rockfill-clay dams. And as a result, even during intense shaking nonlinearities are not sufficiently large to reduce the sharp near-crest amplifications. This is exactly what the results of our analysis have revealed.

The only other factor that may exert a beneficial depressing influence on mid-crest acceleration is the development of high radiation damping if the dam is founded on soft rock. As it has been explained in 4, excitation by vertically propagating *SH* waves would lead to somewhat reduced amplifications at resonances, if the rock-to-dam velocity ratio is of the order of 5 or less. Then one would expect peak-acceleration amplifications of the order of about 3 or 4 rather than 5, which would still produce peak crest accelerations in excess of about 1 g. At the same time, inhomogeneity, which was *not* accounted for in our study, would tend to further increase crest accelerations and thus partly neutralize the beneficial effect of 'incoherent' excitation'.

5.3.5 Permanent sliding-rolling deformations

The previously outlined (Section 5.2) conventional ('Newmark') procedure for estimating residual deformations is applied in this case to assess the consequences of the predicted high response accelerations. For a trial sliding wedge, this procedure compares the spatially-averaged 'driving' acceleration history, $k_a(t)$, with the critical (yield) acceleration, k_y, which would initiate slippage.

$k_a(t)$ is obtained from the acceleration time histories, $a_i(t)$, of all points, i, within each trial sliding mass:

$$k_a(t) = \frac{\iint a_i(t)\mathrm{d}m}{\iint \mathrm{d}mg} \approx \frac{\Sigma\, a_i(t)m_i}{\Sigma\, m_i g} \qquad (12)$$

where m_i is the mass of the (finite) element i.

Selection of realistic values for the angle of shearing resistance, ϕ, of the rockfill is crucial for estimating k_y. Evidently, ϕ is not a just friction angle but an apparent strength parameter which reflects both friction and dilatancy. The latter depends strong on the mean confining pressure, especially for compacted rockfill. (It is worth noting that, due to dilatanacy, the failure 'surfaces' will only macroscopically be smooth curves and straight lines; looked at a smaller scale they will exhibit fluctuations around the 'mean' nominal lines. In essence, 'rolling' rather than 'sliding' will be the predominant motion of the rocky blocks.)

The rockfill for the construction of the 'M' dam will be obtained from required excavations as well as from quarries, from slightly weathered to fresh rock. Since no laboratory test results were available a range of possible values were selected, utilizing published results for similar materials.

A comprehensive summary of available data on shear strength of rockfill has been presented by Leps[85] and a figure from that paper is reproduced in Fig. 20. The rockfill referred to as having strong particles corresponds to rock cores with compressive strengths of 10 000 to 30 000 psi. No such compressive strengths were available in this case, but in view of the above description of the nature of the parent rock, an upper bound and a lower bound curves are selected as depicted in Fig. 20.

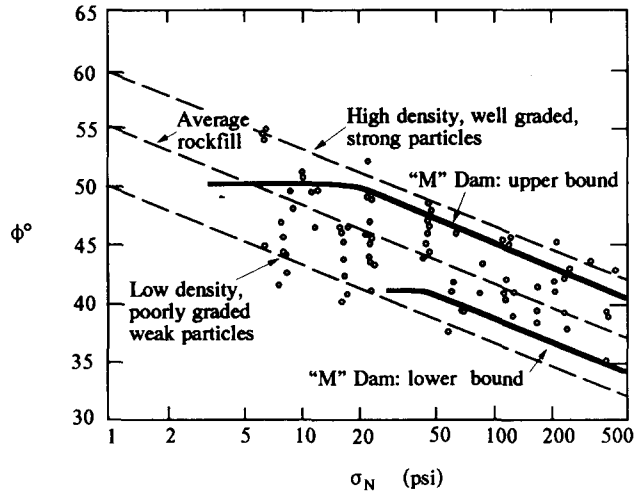

Fig. 20. Angle of shearing resistance of rockfill in large triaxial tests (adapted from Leps[85]).

To utilize these curves, in accordance with the experience from other CFR dams,[27] the distributions of ϕ angles used in the analyses are selected as follows:

(i) The dam is divided into the five zones shown in Fig. 21. These zones are based on estimates of the distribution of confining pressures within the dam. Because of the effect of reservoir loading, the zones are different for maximum pool and minimum pool conditions. The maximum values of mean

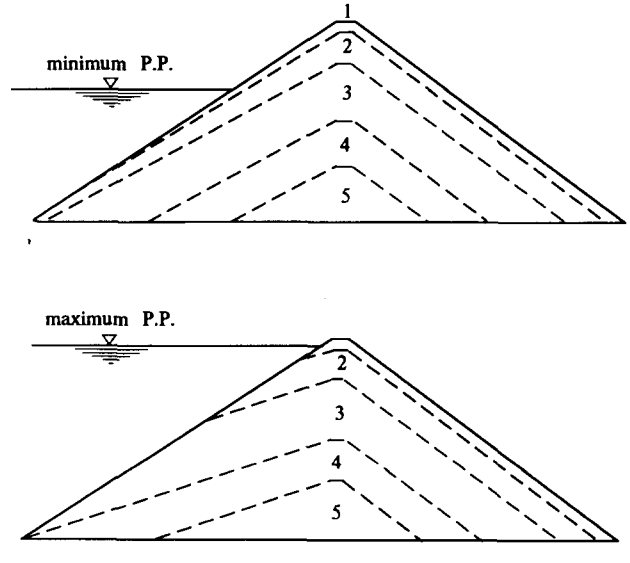

Fig. 21. 'M' dam: zones of different angles of shearing resistance.

octahedral stresses on potential failure planes for zones 1 through 5 are of the order of 100 kPa, 350 kPa, 900 kPa, 1300 kPa, and 1700 kPa.

(ii) Using the foregoing values of mean stress in conjunction with the postulated shear-strength curves of Fig. 20, two sets of discrete values of ϕ are assigned to each zone. For the topmost zone in particular, account is taken of the fact that the upstream material is finer than for the rest of the dam, and that it may be partly saturated (due to leakage) before and during the earthquake shaking. Hence, development of (positive) deleterious pore-water pressures may reduce its cyclic strengths. Furthermore, due to the very low confining pressures in this zone, the strain corresponding to peak strength is small and a substantial reduction in ϕ may occur; use of post-peak values is therefore suggested. Such values may be 5°–10° lower than the peak values for low confining pressures.

A comprehensive parameter study is then performed to compute k_y for a variety of potential slide masses, involving both planar and circular sliding surfaces. More specifically, the infinite-slope approximation, which provides valuable lower bounds for the k_y of thin blocks within the filter and transition upstream zones, leads to a closed-form expression for the yield acceleration. With reference to Fig. 22, k_y is obtained by minimizing the expression for $k_y(\theta)$ which corresponds to an inclination θ of the inertia force:

$$k_y = \min_{\theta} [k_y(\theta)]$$

$$= \min_{\theta} \frac{\sin(\phi - \beta)}{\cos(\phi - \beta - \theta)} = \sin(\phi - \beta) \quad (13)$$

Thus since $\beta = \arctan(1/1{\cdot}4) \approx 35{\cdot}54°$, for shallow failure surfaces with angles of shearing resistance between $40° \leqslant \phi \leqslant 50°$, eqn (13) gives:

$$0{\cdot}08 \leqslant k_y \leqslant 0{\cdot}25 \quad (14)$$

which are very small values. Indeed, even with the unconservative assumption of $\phi = 50°$, the yield accelerations are only a fraction of the peak 'driving' accelerations expected to be induced during the characteristic design earthquake.

Finite planar-wedge and circular sliding surfaces lead to somewhat larger values of k_y. An example of an upstream shallow wedge-type slide extending down to 8 m from the crest, under minimum pool level conditions is shown in Fig. 22. The presence of the crestwall and the retained soil makes such a wedge nearly as vulnerable to inertia forces as the infinite slope is; the resulting yield accelerations are:

$$0{\cdot}10 \leqslant k_y \leqslant 0{\cdot}28 \quad (15)$$

Having determined the critical (yield) acceleration, k_y, and the driving acceleration, $k_a(t)$, of a potential slide

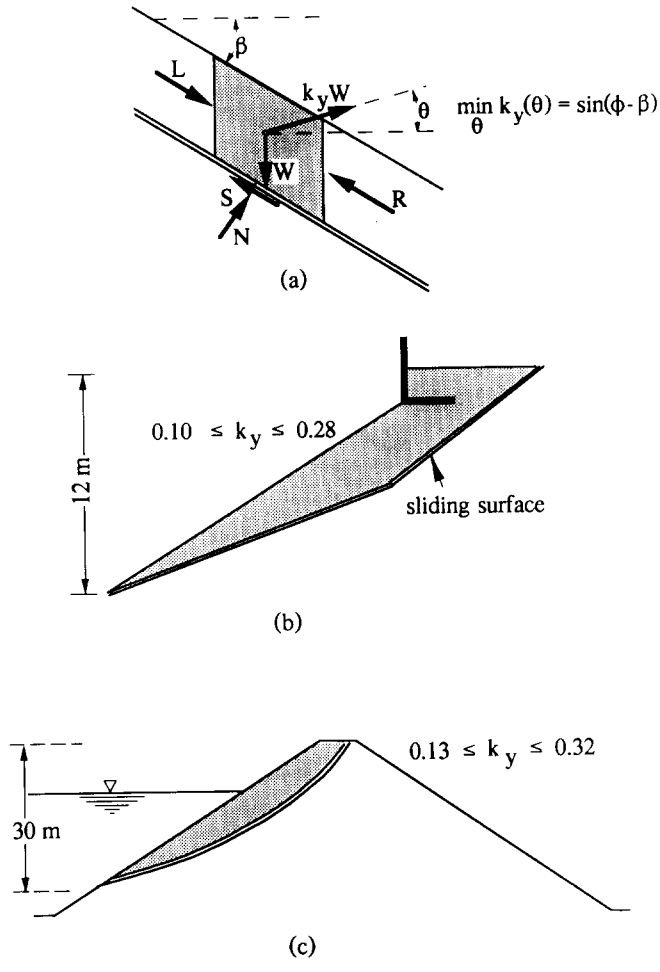

Fig. 22. Three characteristic trial sliding wedges.

mass, nominal sliding displacements, Δ, are estimated by suitably integrating $\delta(t)$, where:

$$\delta(t) = \max([k_a(t) - k_y], 0) \quad (16)$$

Alternatively, Δ can be estimated from published correlations in terms of k_y/K_a.[73,87,88,171]

The nominal sliding displacements Δ along various sliding surfaces are finally combined to obtain rough estimates of the expected settlement of the crest and distortion of the concrete face slab. To determine settlements, the vertically-downward component, Δ_z, of the motion of each sliding mass is computed from Δ:

$$\Delta_z \approx \Delta \cos\beta (1 + \tan\theta \cdot \tan\beta) \quad (17)$$

where β = the angle (with respect to the horizontal) of the direction of sliding — taken as the average angle of the failure surface; and ϕ = the pertinent average angle of shearing resistance along the failure surface. The crest settlements in particular are estimated from the above expression with

$$\Delta \approx \Delta^{us} + \Delta^{ds} \quad (18)$$

where Δ^{us} and Δ^{ds} = the displacements of an upstream and of a downstream sliding wedge, both of which contain the crest.

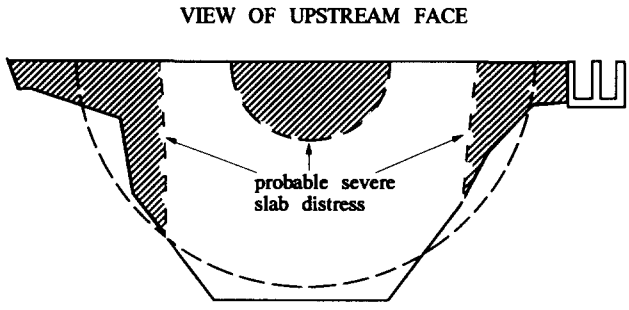

Fig. 23. 'M' dam: zones of predicted most intense damage.

The results for the largest permanent deformations Δ and crest settlements Δ_Z^{crest} are summarized as follows:

(a) $0{\cdot}60\,m < \Delta < 2{\cdot}0\,m$
within the upper (1/10)H from the crest;
(b) $0{\cdot}20\,m < \Delta < 0{\cdot}80\,m$
within the upper (1/3)H from the crest;
(c) $1{\cdot}2\,m\ \Delta_Z^{crest} < 3{\cdot}5\,m$

where the upper-bound values correspond to the most unfavorable, but not unlikely, conditions (lower-bound strength parameters and a slightly conservative choice of seismic excitation).

5.3.6 Potential consequences of seismic response and permanent displacements — suggested design modifications

There is very little actual experience regarding the consequences of such (large) sliding deformations. The advocates of CFR dams[27] argue that displacements of 1-2 meters do not pose any threat on their overall integrity, and an increased free-board is all that is needed to accommodate such crest settlements.

However it can also be convincingly argued that the concentration of sliding-wedge deformations near the upper fourth of the dam (by the midcrest) will imply large distortions of the slab. Hence, in the dark-shaded region depicted in Fig. 23, severe cracking of the concrete slab and 'failure' of the slab joints are very probable during the design earthquake. The economic, in addition to safety, aspects of such a performance deserve careful assessment.

To minimize such problems, several ideas for improvement come to mind:

- Flatten the slopes to at least 1 : 1·55. As mentioned earlier, Seed *et al.*[152] have made a similar recommendation for CFR dams subjected to moderate and strong earthquakes, despite the fact that they only studied an ∞-long dam, i.e. without the deleterious effect of 'wave focusing' in narrow canyons. Alternatively, a 1 : 1·4 slope should change to 1 : 1·6 for the top H/3 of the dam.
- The concrete should be made as ductile as possible. The filter zone should be properly compacted and made sufficiently permeable so that no accumulation of pore water is possible; otherwise the material may become saturated and pore pressures may build up, leading to further reduction in strength and greater deformations. The joints and their waterstops should be properly designed and meticulously constructed to safely (or with minimum damage) undergo large distortions.
- Increase the freeboard by one or two meters and the crest width by at least five meters.

Furthermore, the crest retaining wall is undoubtedly a very vulnerable feature of the 'M' dam. Subjected to lateral accelerations of the order of 1·50 g and vertical accelerations of about 0·40 g, the backfill and the underlying rockfill are likely to sustain considerable loss of apparent strength — a process recently given the name 'fluidization' by Richards *et al.*[130] The critical acceleration k_h^* at which 'fluidization' takes place is simply

$$k_h^* = (1 - k_v)\tan\phi = (1 - 0{\cdot}40)\tan 50° \approx 0{\cdot}72 \tag{19}$$

a value which is only 1/2 of the peak k_h and which is likely to be exceeded several times during the earthquake shaking.

When eqn (19) applies, the angle α of the Coulomb sliding wedge becomes zero, active and passive earth forces become equal, and the soil can no longer sustain any further shear.[131] Consequently, large permanent deformations (translational and rotational) of the wall are almost certain to take place. (Indicative of the vulnerability of crest walls is the reported collapse of the parapet wall on top of the Douhe dam, in China, during the 1976 Tangshan earthquake.)[153]

A redesign of the whole crest is therefore a necessity. Applications and new concepts must be explored; avoiding the wall altogether appears to have distinct benefits.

Finally, longitudinal and vertical oscillations of the dam during the Design Earthquake produce significant tensile and shearing strains at the dam-abutment interface, the consequences of which on the plinth-slab connection deserve an investigation.

5.3.7 Conclusion

Concrete-Faced Rockfill (CFR) Dams are widely considered capable of withstanding strong earthquake ground shaking, although no actual CFR dam has up to now been subjected to such shaking. On the other hand, our analyses have unveiled that tall CFR Dams in very narrow canyons of solid rock may experience extremely intense near-crest shaking during significant seismic events — a direct consequence of their very stiff and unyielding structure. The overall integrity of the dam may still not appear to be in danger. However, some rather significant deformation problems are likely to occur: nonuniform permanent distortions; cracking of and leakage through the concrete slab, settlement of the

crest and decrease of the available free-board, and failure of the crest retaining wall. All this would, at the very least, disrupt the functioning of the facility and necessitate expensive repairs. Some modifications in current design practice are therefore needed to alleviate such problems and improve the seismic reliability of CFR dams.

6 ASEISMIC DESIGN CONSIDERATIONS — DEFENSIVE MEASURES

Whenever analysis predicts unsatisfactory performance design actions are necessary. Seed[142,150] pointed out the need for some 'commonsense' defensive measures that would either reduce the risk of failure or assure that the consequences of failure are tolerable. Moreover, it is clear that even sophisticated and elaborate analyses can not provide all the answers; therefore, engineering judgement guided by experience is needed for a reliable design of an earth or rockfill dam. Adopting arguments from Marcuson & Franklin,[94] we may state that 'defensive design' measures serve:

- to provide protection against hazards that are recognized but cannot be possibly or easily analyzed
- to mitigate harmful effects for which analysis can only provide indirect qualitative evidence
- to provide a second line of defense against unforseen damaging actions such as cracking and piping.

Among the defensive measures listed by Seed[142] we mention: the provision for ample freeboard to allow for settlement and slumping; the design of wide filters and transition zones of material not vulnerable to cracking; and the use of plastic material for earth cores to minimize cracking. The presentation of Marcuson & Franklin[94] on the other hand focused on design actions primarily against liquefaction in new and existing embankment dams.

Modern methods of analysis (such as those described in this paper) can increase our awareness of potential problems and help us find appropriate defensive measures. They can also be used to evaluate the likely effectiveness of any proposed action on the original design — although probably only in qualitative terms, despite the progress in the state-of-the-art. The final decision will inevitably call for engineering judgement helped and guided by analysis and experience.

In the sequel we outline only a few design rules and defensive measures for which there is at least partial analytical justification. Application of these rules is illustrated for both Earth-Core Rockfill (ECR) and Concrete-Faced Rockfill (CFR) dams. Some of the presented ideas have already been introduced in Section 5.3.6 as required modifications in the original design of the 'M' dam case study. Reference is made to Kutzner[82] for a more comprehensive discussion of the application of basic design rules to earth and rockfill dams.

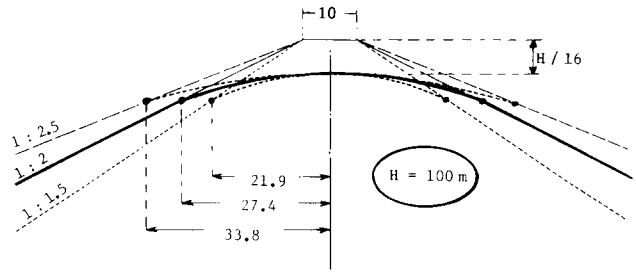

Fig. 24. Curved crest shape proposed by Baba[14].

6.1 Crest and slopes (in ECR and CFR Dams)

The demand for widening the crest and flattening the slopes follows from the observed and computed increased acceleration levels near the top of the dam. The 'tower' or 'whip-lash' effect, demonstrated in Figs 16–17, would initiate local slides, especially when crest accelerations approach or exceed 1 g. Thus, to compensate for the resulting slumping, a 20 m crest width was considered necessary for the 160 m Chico, Philippines, ECR dam (slopes 1 : 1·85) designed against earthquake shaking expected to produce peak crest acceleration of about 1 g.[82] But more moderate width increases in combination with other defensive measures are adopted in most dams.

To avoid crest slumping, Bolognesi[18] and Seed *et al.*[152] have advocated the adoption of a flatter slope near the crest and a steeper slope in the lower part of the dam, rather than using a uniform slope throughout the full height. This concept seems to have particular merit for CFR dams, especially if they are to be built in narrow canyons and supported by competent rock. As explained in 5, in such a case accelerations can be very high only at the top 1/4 of the dam, where at least two unfavorable conditions prevail: (i) the benefit of the 'confining' reservoir water may be only partially (if at all) available; and (ii) the added weight of the crest retaining wall reduces the available static margin of safety of shallow sliding wedges (recall Fig. 22).

Baba[14] has extended the foregoing 'variable-slope' concept. Using small-scale shaking-table experiments and analytical studies as a guide, he proposed that the top of the dam be shaped as a parabolic curve, as sketched in Fig. 22. Such a shape would undoubtedly minimize sliding deformations, but at the expense of increased volume of rockfill.

An economic alternative to excessive flattening of the near-crest slopes is to change the composition of the zone where accelerations in excess of 0·75 g are predicted. Seed *et al.*[152] recommended placing *compacted clayey and sand and gravel* instead of rockfill or compacted gravel, in order to 'eliminate arguments about the behavior of cohesionless material in this zone of the embankment'; because it is 'cohesive soils that are known to be able to withstand such high accelerations without detrimental deformations'. (cit.).

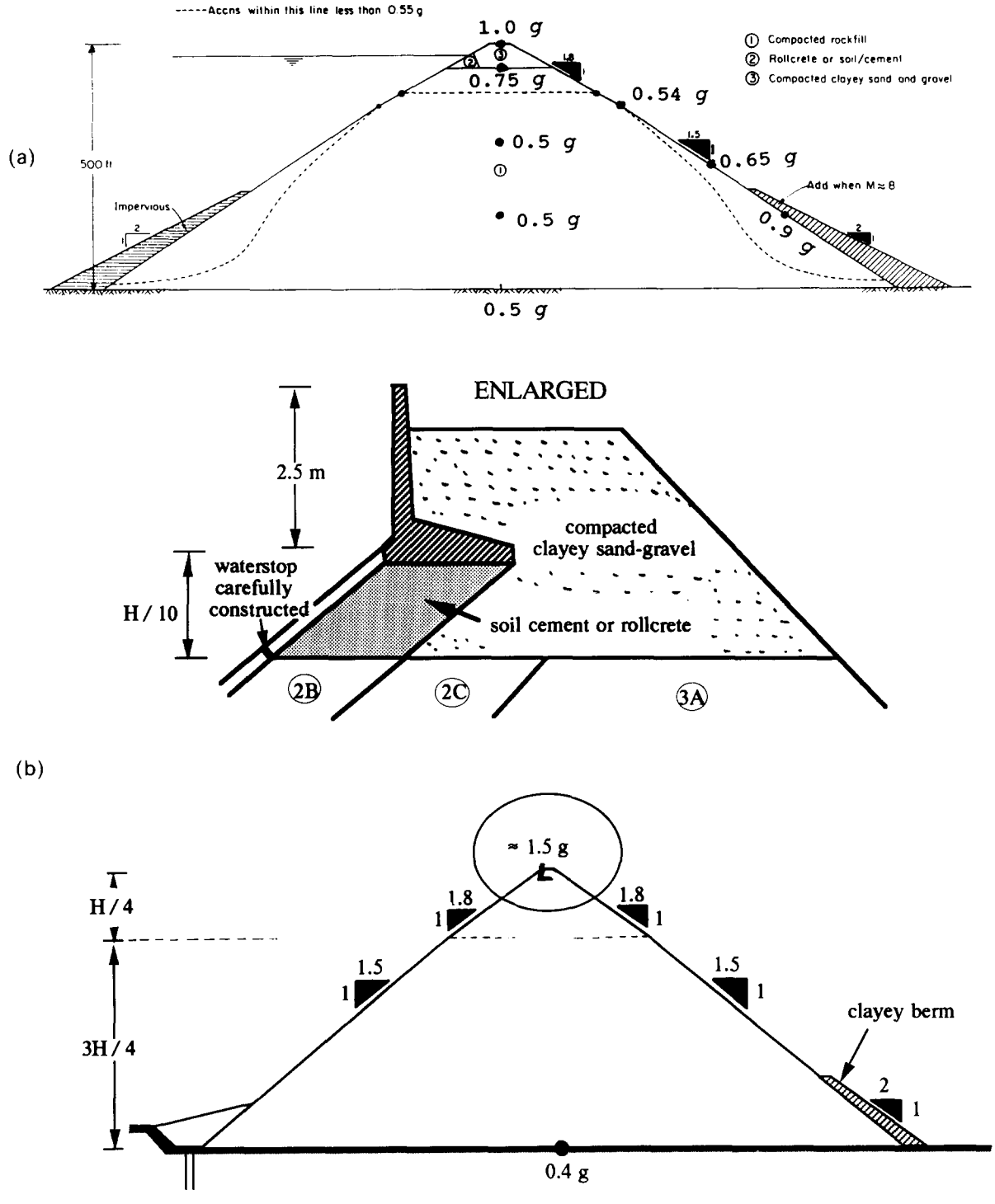

Fig. 25. Two conceptual sections for CFR dam under very strong seismic shaking: (a) for a dam in a wide canyon (Seed *et al.*[152]); (b) for a dam in a narrow rigid canyon (authors).

For CFR dams in particular, when near-crest accelerations are predicted to exceed 1 g, *soil cement or rollcrete* may be placed on the upstream part of this zone. In addition to being economical (especially if sound durable rock is not readily available at or close to the site) soil cement would also offer support to the crest retaining ('parapet') wall, the vulnerability of which was documented in Section 5.36. Of course, additional measures may be necessary to minimize deformations of the crest walls, including a limit on their height to no more than 2–3 meters (whereas the current trend is for 5–6 meters high walls), accompanied with an increased footing.

Dynamic finite-element analyses often show that zones of very high accelerations develop (during long-duration strong shaking) near the lower outer portions of the shells, i.e. in Fig. 25(a) at the bottom third by the two

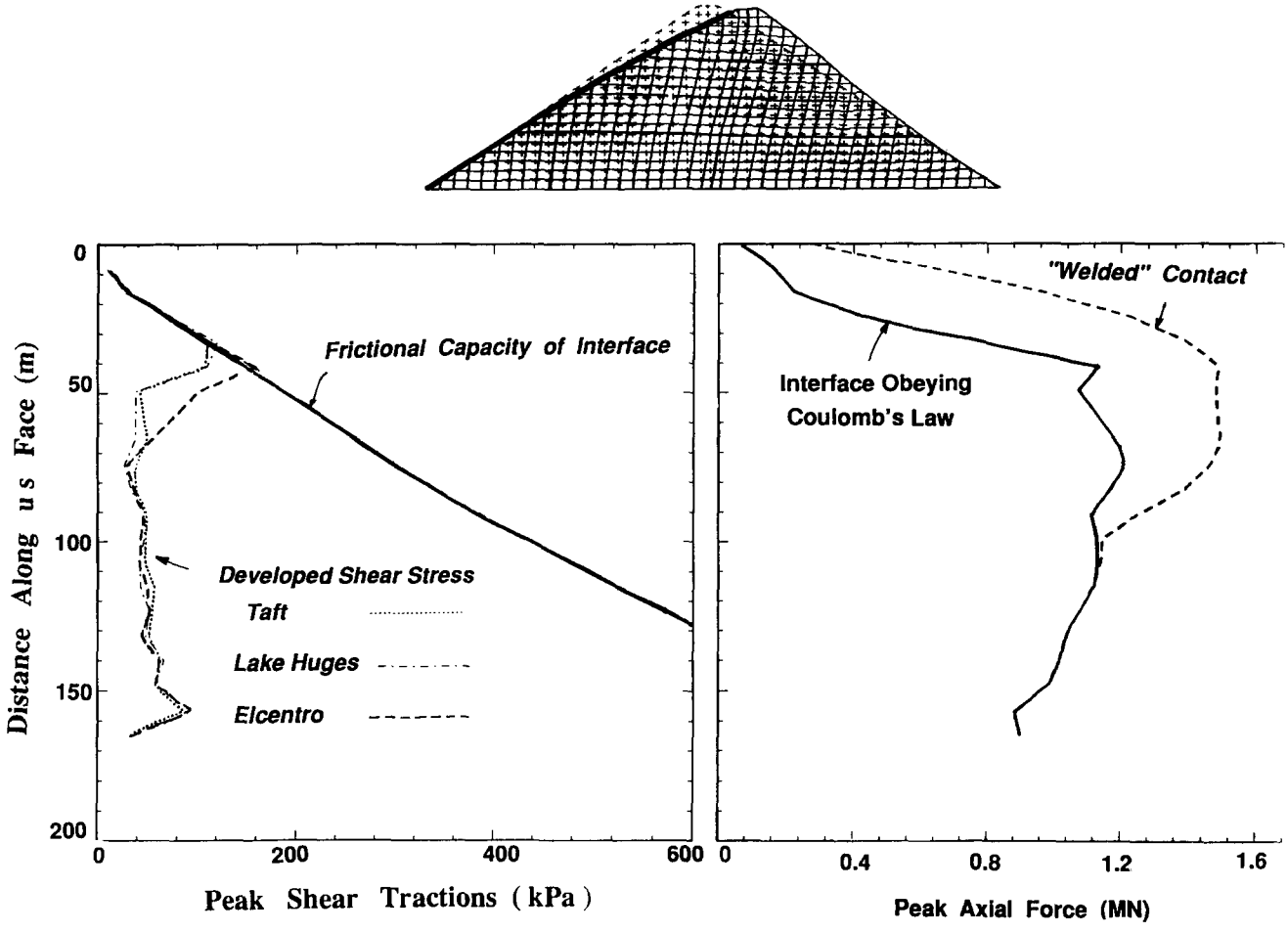

Fig. 26. Preliminary results for an 100 m-tall plane (2D) model of a CFR dam subjected to strong (0·40 g) excitation: top, F.E. mesh and fundamental mode shape; left, distribution of shear tractions that develop at the face slab–soil interface; right, distribution of peak values of axial force in the face slab.

faces of the dam. Seed *et al.*[152] suggest the placement of stabilizing impervious berms on both slopes. For CFR dams an upstream such berm is not needed for stability, in view of the beneficial high reservoir-water pressures; nevertheless an impervious fill is often just placed there to minimize leakage under the plinth and through the waterstops of the plinth-slab perimetric joint.

The above ideas are portrayed in Fig. 25 through two conceptual sections of CFR dams (both 150 m high) in a highly seismic region where the design high-magnitude event is expected to induce peak crest accelerations of 1.0 g and 1.5 g, respectively.

6.2 Face slab and supporting zone (in CFR dams)

Presently, there is hardly any analytical or observational evidence on the behavior of concrete face slabs during strong seismic shaking. The choice of slab thickness and steel reinforcement is based solely on precendent, and performance under static loads is the only consideration. Yet, even when the dam undergoes elastic-type seismic deformations the tensile axial forces in the slab may exceed the capacity of concrete in tension and would thereby initiate cracking. As an example, Fig. 26 presents 2D results for the dynamic behavior of the face slab of an idealized 100 m CFR dam section subjected to three historic accelerograms, all scaled to a 0·40 g peak acceleration. The linear viscoelastic analyses were performed with a standard F.E. code, in which the slab-rockfill interface was assumed to either be in full ('wedded') contact, or to obey Coulomb's friction law. From the distribution of the peak values of the shear tractions developing between slab and supporting soil it is seen that the frictional capacity of this interface is mobilized only in the upper fifth of the slab, where of course the confining water pressures are not substantial. The resulting peak values of the axial force in the slab (average of the three analyses) reach values of about 1 MN. Evidently, a 0·40 m thick slab would experience stresses only slightly exceeding the tensile strength (≈ 2 MPa) of the concrete along most of the face. However, the inelastic sliding-wedge type of deformations near the upper fourth of the dam will likely impose large (concentrated? . . .) distortions on the slab, far beyond what the equivalent linear analysis suggests. The consequences are likely to be: severe cracking of the

concrete and failure of inadequate construction joints. No method is presently available to realiably predict the occurrence of such deformations.

Possible measures that would mitigate the foregoing effects: making the reinforced concrete strong and ductile; and allowing for a number of horizontal joints with carefully designed and constructed waterstops to withstand tension.

The important role of the upstream zone on which the slab rests has already been undressed in 5.1. The proposition by Sherard[155] to change the current practice by increasing from about 20% to 40% or more the percentage of particles passing the No. 4 sieve, remains in our opinion controversial. The likelihood that part of this zone of cohesionless material would be saturated when strong ground motions excite the dam is a valid argument against that increase. This is so because such a material would be of too low permeability (between 10^{-5} and 10^{-6} m/s) to allow drainage of water 'normally' leaking through the concrete face or any defective waterstops, or even through cracks inflicted from a foreshock or an earlier earthquake.

Concluding, we would like to emphasize the need for field data on the basis of which to judge the merits of the various design concepts and defensive measures against strong shaking. Planning for the collection of such data should be given first priority.

ACKNOWLEDGEMENTS

The research of the authors has been sponsored by the US National Science Foundation through Grants No. CEE-8205345 and ECE-8413472. Mr Ke Fan, student at SUNY, Buffalo, provided considerable help with the artwork.

REFERENCES

1. Abdel-Ghaffar, A.M., & Scott R.F. Analysis of earth dam response to earthquakes, *J. of the Geotech. Engrg. Div.*, ASCE, 1979, **105,** No. GT12, 1379–1404.
2. Abdel-Ghaffar, A.M. & Scott, R.F. Shear moduli and damping factors of earth dams, *J. of the Geotech. Engrg. Div.*, ASCE, 1979, **105,** No. GT12, 1405–1426.
3. Abdel-Ghaffar, A.M. & Scott, R.F. Vibration tests of a full-scale earth dam, *J. of the Geotech. Engrg. Div.*, ASCE, 1981, **107,** No. GT3, 241–269.
4. Abdel-Ghaffar, A.M. & Scott, R.F. Comparative study of dynamic response of earth dam, *J. of the Geotech. Engrg. Div.*, ASCE, 1981, No. GT3, 271–286.
5. Abdel-Ghaffar, A.M. & Koh, A.S. Longitudinal vibration of non-homogeneous earth dams, *Earthq. Engrg. & Struct. Dyn.*, 1987, **9**(3), 279–305.
6. Abdel-Ghaffar, A.M. & Koh, A.S. Earthquake induced longitudinal strains and stresses in nonhomogeneous earth dams, *Earthq. Engrg. & Struct. Dyn.*, 1981, **9** (9), 521–542.
7. Abdel-Ghaffar, A.M. & Koh, A.S. Three-dimensional dynamic analysis of nonhomogeneous earth dams, *Soil. Dyn. & Earthq. Engrg.*, 1982, **1**(3), 136–144.
8. Abdel-Ghaffar, A.M. & Elgamal, A.W.M. Elasto-plastic seismic response of 3-D earth dams: theory, *J. of the Geotech. Engrg. Div.*, ASCE, 1987, **113**(11), 1293–1308.
9. Aki, K. & Larner, K. Surface motion of a layered medium having an irregular interface due to incident plane *SH* waves, *J. of Geophysical Research*, 1970, **75,** 933–954.
10. Ambraseys, N.M. On the shear response of a two-dimensional wedge subjected to an arbitrary disturbance, *Bulletin of the Seismol. Soc. of America*, 1960, **50,** 45–46.
11. Ambraseys, N.M. The seismic stability of earth dams, *Proc. of the 2nd World Conf. on Earthq. Engrg.*, Tokyo, 1960, **3,** 1345–1363.
12. Ambraseys, N.M. & Sarma, S.K. The response of earth dams to strong earthquakes, *Geotechnique*, **17,** 181–213.
13. Arrau, L., Ibarra & Nogurea, G. Concrete face rockfill dams design, construction and performance, ASCE at Detroit, Michigan, 1985.
14. Baba, K. Proposal of a countermeasure for earthquake resistant design of dam, *Proc. of Ninth World Conf. on Earthq. Engrg.*, 1988, Vol. VI, Tokyo-Kyoto, Japan.
15. Bard, P. & Bouchon, M. The seismic response of sediment-filled valleys. Part I. The case of incident *SG* waves, *Bulletin of Seismol. Soc. of America*, 1980, **70**(4), 1263–1286.
16. Bard, P. & Bouchon, M. The seismic response of sediment-filled valleys. Part 2. The case of incident *P* & *SV* waves, *Bulletin of Seismol. Soc. of America*, 1980, **70**(5), 1921–1941.
17. Bard, P. & Bouchon, M. The two-dimensional resonance of sedimentary-filled valleys, *Bull. of Seismol. Soc. of America*, 1985, **75,** 519–541.
18. Bolognesi, A.J.L. Peculiarities of the seismic-resistant analysis of earth dams with pervious gravelly shells, *Design of Dams to Resist Earthquake*, ICE, London, 1980, 75–82.
19. Boore, D.M. Stochastic simulation of high-frequency ground motions based on seismological models of the radiated spectra, *Bulletin of the Seismol. Soc. of America*, 1983, **73**(6), 1856–1894.
20. Bravo, M.A. & Sanchez-Sesma, F.J. Seismic response of alluvial valleys for incident *P*, *SV* & Rayleigh waves, *J. of Soil Dyn. & Earthq. Engrg.*, 1990, **9**(1), 16–19.
21. Bureau, G. Volpe, R.L., Roth, W. & Udaka, T. Seismic analysis of concrete face rockfill dams, *Concrete Face Rockfill Dams — Design, Construction and Performance*, ASCE, 1985, 479–508.
22. Campbell, K.W. Predicting strong ground motion in Utah, Evaluation of regional & urban earthquake hazards in Utah, USGS Prof. Paper, 1988.
23. Casinader, R. Discussion on the upstream zone in CFR dams, by J.L. Sherard, *J. Geotech. Engineering*, ASCE, 1987, **113**, 1231–1234.
24. Charles, J.A. & Soares, M.M. Stability of compacted rockfill slopes, *Geotechnique*, 1984, **34,** 61–70.
25. Clough, R.W. & Chopra, A.K. Earthquake stress analysis in earth dams, *J. of the Engrg. Mech. Div.*, ASCE, 1966, **92**(EM2), 197–211.
26. Constantinou, M.C. & Gazetas, G. Stochastic seismic sliding of rigid mass against asymmetric Coulomb friction, *Earthq. Eng. and Struct. Dyn.*, 1984, **12,** 777–793.
27. Cooke, J.B. & Sherard, J.L., eds. *Concrete Face Rockfill Dams — Design, Construction & Performance*, ASCE publication, 1985, pp. 656.
28. Cooke, J.B. & Sherard, J.L. Concrete-face Rockfill Dam: II Design, *J. Geotech. Engrg.*, ASCE, 1987, **113**(10), 1113–1139.
29. Dakoulas, P. & Gazetas, G. Nonlinear response of

embankment dams, *Proc. 2nd Int. Conf. Soil Dyn. and Earthq. Engr.*, June/July, Springer-Verlag, 1985, **5**, 29–44.
30. Dakoulas, P. & Gazetas, G. A class of inhomogeneous shear models for seismic response of dams and embankments, *Soil Dyn. & Earthq. Engrg.*, 1985, **4**(4), 166–182.
31. Dakoulas, P. & Gazetas G. Seismic shear vibration of embankment dams in semi-cylindrical valleys, *Earthq. Engrg. & Struct. Dyn.*, 1985, **14**, 19–40.
32. Dakoulas, P. & Gazetas, G. Seismic shear strains and seismic coefficients in dams and embankments, *Soil Dyn. & Earthq. Engrg.*, 1986, **5**(2), 75–83.
33. Dakoulas, P. Nonlinear response of dams founded on alluvial deposit in narrow canyons, *Int. J. of Soil Dyn. & Earthq. Engrg.*, 1991, **9**(6), 301–312.
34. Dakoulas, P. & Hashmi, H. Response of earth dams in canyons subject to asynchronous base excitation, *Second International Conf. of Geotech. Earthq. Engrg. & Soil Dyn.*, St. Louis, Vol. II, 1105–1112.
35. Dibaj, M. & Penzien, J. Response of earth dams to traveling seismic waves, *J. Soil Mech. & Found. Div.*, ASCE, 1969, **95**, SM2.
36. Dungar, R. Computer modelling of embankment dams: response to earthquake, *Water Power and Dam Construction*, 1990.
37. Earthquake Engineering Technology, Inc. SuperFLUSH Version 3.2, 1985.
38. Elgamal, A.W.M. Near earthquake-response analysis of earth dams, Ph.D. Thesis, Dept. of Civil Engrg., Princeton University, Princeton, N.J., 1985.
39. Elgamal, A.W.M., Abdel-Ghaffar, A.M. & Prevost, J.H. Elasto-plastic earthquake shear response of one-dimensional earth dam models, *Earthq. Engrg. & Struct. Dyn.*, 1985, **13**, 617–633.
40. Elgamal, A.W. Shear hysteretic elasto-plastic earthquake response of soil systems, *J. of Earthq. Engrg. & Struct. Dyn.*, 1991.
41. Elgamal, A.W.M., Abdel-Ghaffar, A.M. & Prevost, J.H. 2-D elastoplastic seismic shear response of earth dams: theory, *J. of the Engrg. Mech. Div.*, ASCE, 1987, **113**(5), 689–701.
42. Elgamal, A.W.M. & Abdel-Ghaffar, A.M. Elasto-plastic seismic response of 3-D earth dams: applications, *J. of the Geotech. Engrg. Div.*, ASCE, 1987, **113**(11), 1309–1325.
43. Elgamal, A.W.M., Scott, R.F., Succarieh, M.F. & Yan, L.P. La Villita dam response to five earthquakes including permanent deformation, *J. Geotech. Engrg.*, ASCE, 1990, **116**(10).
44. Fedock, J.J. Modal responses of a large earth and rockfill dam, *Proc. of IX World Conf. on Earthq. Engrg.*, Vol. VI, Tokyo-Kyoto, Japan, 1988.
45. Fedock, J.J. Analysis of strong-motion earthquake records from a well-instrumented earth dam, 1980.
46. Finn, W.D.L., Yogendrakumar, M., Yoshida, N. & Yoshida, H. TARA-3: a program to compute the response of 2D embankments and soil-structure interaction systems to seismic loading, Univ. of British Columbia, Vancouver, Canada, 1986.
47. Finn, W.D.L. Dynamic analysis in geotechnical engineering, *Earthq. Engrg. & Soil Dyn. II*, ASCE, 1988, 523–592.
48. Finn, W.D.L. Assessment of liquefaction potential and postliquefaction behavior of earth structures: developments 1981–1991, *Proc. 2nd Int. Conf. on Recent Advances in Geotech. Earthquake Engrg. & Soil Dynamics*, St. Louis, 1991, Vol. II, pp. 1833–1850.
49. Fitzpatrick, M., Cole, B., Kinstler, F. & Knoop, B. Design of concrete-faced rockfill dams, *Concrete Face Rockfill Dams — Design, Construction and Performance*, ASCE, 1985, 410–434.
50. Franklin, A.G. & Chang, F.K. Earthquake resistance of earth and rock-filled dams, Rep. 5: permanent displacements of earth embankments by Newmark sliding block analysis, Misc. Pap. S-71-17, USAE Waterways Experimental Station, Vicksburg, MS, 1977.
51. Gazetas, G. Longitudinal vibrations of embankment dams, *J. of the Geotech. Engrg. Div.*, ASCE, 1981, **107**, GT1, 20–40.
52. Gazetas, G. A new dynamic model for earth dams evaluated through case histories, *Soils & Foundations, J. of the Japan. Soc. for Soil Mech. & Found.*, 1981, **21**(1), 29–40.
53. Gazetas, G. Vertical oscillation of earth and rockfill dams: analysis and field observation, *Soils & Foundations, J. of the Japan. Soc. for Soil Mech. & Found.*, 1981, **21**(4), 265–277.
54. Gazetas, G., Debchaudhury, A. & Gasparini, D.A. Random vibration analysis for the seismic response of earth dams, *Geotechnique*, 1981, **31**(2), 261–277.
55. Gazetas, G. & Abdel-Ghaffar, A.M. Earth dam characteristics from full-scale vibration, *Proc. of the X Int. Conf. on Soil Mech. & Found. Engrg., Stockholm*, 1981, Vol. 3, pp. 207–210.
56. Gazetas, G. Shear vibrations of vertically inhomogeneous earth dams, *Int. J. for Numerical & Analytical Methods in Geomech.*, 1982, **6**(1), 219–241.
57. Gazetas, G., Debchaudhury, A. & Gasparini, D.A. Stochastic estimation of the non-linear seismic response of earth dams, *International J. of Soil Dyn. & Earthq. Engineering*, 1982, **1**(1), 39–46.
58. Gazetas, G. Seismic response of earth dams: some recent developments, *Soil Dyn. & Earthq. Engrg.*, **6**(1), State-of-the-Art issue, 1–47. (Presented at the 2nd Int. Conf. on Soil Dyn. & Earthq. Engineering, 1985.)
59. Gazetas, G. Seismic analysis of concrete face rockfill dams, discussion, *J. of Geotech. Engineering*, ASCE, 1987, **113**(10), 1247–1251.
60. Ghaboussi, J. & Dikmen, S.U. Liquefaction analysis of horizontally layered sands, *J. of the Geotech. Engrg. Div.*, 1978, **104**, No. GT3, 341–356.
61. Geli, L., Bard, P. & Jullien B. The effect of topography on the earthquake ground motion: a review and new results, *Bulletin of Seismol. Soc. of America*, 1988, **78**(1), 42–63.
62. Griffiths, D.V. & Prevost, J.H. Two- and three-dimensional dynamic finite element analyses of the Long Valley dam, *Geotechnique*, 1988.
63. Guros, F.B., Thiers, G.R., Wathen, T.R., & Buckles, C.E. Seismic design of concrete-faced rockfill dams, *Proc. of 8th World Conf. on Earthq. Engrg.*, San Francisco, CA, 1984, Vol. III, pp. 317–323.
64. Hall, J.F. & Chopra, A.M. Effects in earthquake response of embankment dams, *J. of the Geotech. Engrg. Division*, ASCE, 1982, **108**, No. GT4, 591–597.
65. Han, G., Kong, X. & Li, J. Dynamic experiments and numerical simulations of model concrete-faced rockfill dams, *Proc. of IX World Conf. on Earthq. Engrg.*, Vol. VI, 1988, Tokyo-Kyoto, Japan.
66. Hanks, T.C. & McGuire, R.K. The character of high frequency strong ground motion, *Bull. Seismol. Soc. of America*, 1981, **71**, 2071–2905.
67. Hashmi, H. Response of earth dams in canyons subjected to asynchronous base excitation, M.S. Thesis, Rice University, Houston, Texas, 1989.
68. Hatanka, M. Three dimensional consideration on the vibration of earth dams, *J. of the Japan. Soc. for Civil Engrg.*, Tokyo, 1982, **37**(10), 1–6.
69. Hatanka, M. Fundamental considerations on the earthquake resistant properties of the earth dam, *Disaster*

Prevention Research Institute, Bulletin No. 11, Kyoto University, Japan, Dec., 1955, pp. 1–36.
70. Hayashi, M., Komada, H. & Fujiwara, Y. Three dimensional dynamic response and earthquake resistant design of rock fill dam against input earthquake in direction of dam axis, *Proc. of the 5th World Conf. on Earthq. Engrg.*, Rome, 1973, **2**(189).
71. Hirata, K. & Shinozuka, M. Stochastic analysis of seismic stability of earth dams, *Proc. of Ninth World Conf. on Earthq. Engrg.*, 1988, Vol. VI, Tokyo-Kyoto, Japan.
72. Hynes, M.E. Pressure generation characteristics of gravel under undrained cyclic loading, Ph.D. Dissertation, Univ. California, Berkeley, 1988.
73. Hynes-Griffin, M.E. & Franklin, A.G. Rationalizing the seismic coefficient method, USAE Waterways Experiment Station, Misc. Paper GL-84-13, Vicksburg, MS, 1984.
74. Idriss, I.M. Evaluating seismic risk in engineering practice, *XI Int. Conf. on Soil Mech. & Found. Engineering*, 1985, Vol. 1, pp. 255–320.
75. Idriss, I.M. & Seed, H.B. Seismic response of horizontal soil layers, *J. of Soil Mech. & Found. Div.*, ASCE, 1968, **94**(SM4), 1003–1031.
76. Idriss, I.M., Lysmer, J., Hwang, R. & Seed, H.B. QUAD-4: a computer program for evaluating the seismic response of soil-structures by variable damping finite element procedures, Report No. EERC 73-16, Univ. of California, Berkeley, California, July, 1983.
77. Ishihara, K. Stability of natural deposits during earthquakes, *Proc. of 11th Int. Conf. on Soil Mech. & Found. Engineering*, San Francisco, 1985, Vol. 1, pp. 321–376.
78. Ishizaki, H. & Hatakeyama, N. Considerations on the vibrational behaviors of earth dams, *Disaster Prevention Research Inst., Bulletin No. 52*, Kyoto, Japan, 1962.
79. Kawai, T. Summery report on the development of the computer program DIANA — Dynamic Interaction Approach and Non-Linear Analysis, Science Univ. of Tokyo, 1985.
80. Kawase, H. Time-domain response of a semi-circular canyon for incident *SV*, *P* and Rayleigh waves calculated by the discrete wave number boundary element method, *Bull. of Seismol. Soc. of America*, 1988, **78,** 1415–1437.
81. Kokusho, T. & Esashi, Y. Cyclic triaxial test of sands and coarse materials, *Proc. of X World Conf. on Soil Mech. & Found. Engrg.*, Stockholm, 1981.
82. Kutzner, C. Design and construction of earthquake-resistant earth and Rockfill dams, *Geotech. Engrg.*, Bangkok, 1985, **16,** 1–24.
83. Lacy, S.J. Numerical procedures for nonlinear transient analysis of two-phase soil systems, Ph.D. Thesis, Dept. of Civil Engrg., Princeton University, Princeton, NJ, 1986.
84. Lacy, S.J. & Prevost, J.H. Nonlinear seismic response analysis of earth dams, *Soil Dyn. & Earthq. Engrg.*, 1987, **6**(1), 48–63.
85. Leps, T.M. Review of shearing strength of rockfill, *J. Soil Mech. & Foundations Div.*, ASCE, 1970, **96,** No. SM4.
86. Lin, J.S. & Whitman, R.V. Decoupling approximations to the evaluation of earthquake-induced plastic slip in earth dams, *Earthq. Engrg. & Struct. Dyn.*, 1983, **11,** 667–678.
87. Lin, J.S. & Whitman, R.V. Earthquake induced displacements of sliding blocks, *J. of Geotech. Engineering Div.*, ASCE, 1986, **112**(1), 44–49.
88. Makdisi, F.I. & Seed, H.B. Simplified procedure for estimating dam and embankment earthquake-induced deformations, *J. of the Geotech. Engrg. Div.*, ASCE, 1987, **104,** GT7, 849–867.
89. Makdisi, F.I. & Seed, H.B. Simplified procedure for evaluating embankment response, *J. of the Geotech. Engrg. Div.*, ASCE, 1979, **105,** GT12, 1427–1434.
90. Makdisi, F.I., Kagawa, T. & Seed, H.B. Seismic response of earth dams in triangular canyons, *J. of the Geotech. Engrg. Div.*, ASCE, 1982, **108,** GT10, 1328–1337.
91. Mansuri, T.A. & Nelson, J.D. Dynamic response and liquefaction of earth dams, *J. Geotech. Engrg.*, ASCE, 1983, **109**(1) 89–100.
92. Martin, G.R. The response of earth dams to earthquakes, Ph.D. Thesis, Univ. Calif., Berkeley, 1965.
93. Marcuson, W.F., III & Krinitzsky, E.L. Dynamic analysis of Fort Peak Dam, Waterways Experiment Station Report S-76-1, Vicksburg, 1976.
94. Marcuson, W.F., III & Franklin, A.G. Seismic design, analysis and remedial measures to improve stability of existing earth dams — corps of engineers approach, *Seismic Design of Embankments & Caverns*, ASCE, 1983, 65–78.
95. Marcuson, W.F., III, Hynes, M.D. & Franklin, A.G. Evaluation and use of residual strength in seismic safety analysis of embankments, *Earthquake Spectra*, 1990, **6**(3), 529–572.
96. Martin, G.R., Finn, W.D.L. & Seed, H.B. Fundamentals of liquefaction under cyclic loading, *J. Geotech. Engrg. Div.*, ASCE, 1975, **101,** GT5, 324–438.
97. Martinez, B. & Bielak, T. On the three dimensinal seismic response of earth structures, *Proc. of the Seventh World Conf. on Earthq. Engrg.*, 1980, Vol. 8, Istanbul, pp. 523–528.
98. Matsumoto, N., Yasuda, N. & Shiga M. Dynamic behavior of a Rockfill Dam during earthquakes, Public Works Research Institute, Ministry of Construction.
99. Mathur, J.N. Analysis of the response of earth dams to earthquakes, Ph.D. Thesis, Univ. Calif., Berkeley, 1969.
100. Medvedev, S. & Sinitsym, A. Seismic effects on earth fill dams, *Proc. of 3rd World Conf. on Earthq. Engrg.*, New Zealand, Paper IV/M/18, 1965.
101. Mejia, L.H., Seed, H.B. & Lysmer, J. Dynamic analysis of earth dam in three dimensions, *J. of the Geotech. Engrg. Div.*, ASCE, 1982, **108,** 1586–1604.
102. Mejia, L.H. & Seed, H.B. Comparison of 2D and 3D dynamic analysis of earth dams, *J. of the Geotech. Engrg. Div.*, ASCE, 1983, **109**(11), 1383–1398.
103. Mejia, L.H., Sykora, D.W., Hynes, M.E., Fung, K. & Koester, J.P. Measured and calculated dynamic response of rock-fill dam, *Proc. 2nd Int. Conf. Soil Dyn. & Geotech. Earthq. Engrg.*, St. Louis, 1991, Vol. II, pp. 1063–1070.
104. Mohamad, R., Dakoulas, P., Gazetas, G. & Dorby, R. Liquefaction flow failure evaluation of earth dams, *Proc. XI Conf. Soil Mech. Found. Engrg.*, San Francisco, 1985.
105. Mohamad, R. Evaluation of seismically induced liquefaction flow failure of earth dams, Ph.D., Dissertation, Renssealear Polytechnic Institute, Troy, 1985.
106. Mononobe, N., Takata, A. & Matumura, M. Seismic stability of the earth dam, *Proc. of the 2nd Congress on Large Dams*, Washington, D.C., 1936, Vol. 4, 435–443.
107. Mori, Y. *et al.* Dynamic properties of the Ainono and Usino dams, *J. Jap. Soc. Civ. Engrgs.*, 1975, 240.
108. Morris, M. Design and construction of Teror Lake dam, *Concrete Face Rockfill Dams — Design, Construction and Performance*, ASCE, 362–378.
109. Nahhas, T.M. Dynamics of earth dams, Ph.D. Thesis, Univ. of Southern California, Los Angeles, 1987.
110. Newmark, N.M. A method of computation for structural dynamics, *J. of the Engrg. Mech. Div.*, ASCE, 1959, **85,** EM3, 67–94.
111. Newnark, N.M. Effects of earthquakes on dams and embankments, *Geotechnique*, 1965, **15**(2), 139–160.

112. Nose, M. & Baba, K. Dynamic behavior of rockfill dams, Design of Dams to Resist Earthquake, *ICE*, London, 1980, 55–64.
113. Ohmachi, T. Analysis of dynamic shear strain distributed in three-dimensional earth dam models, *Proc. of the 1st International Conf. on Recent Advances in Geotech. Earthq. Engrg. & Soil Dyn.*, Univ. of Missouri-Rolla, St. Louis, Mo., 1981, pp. 459–464.
114. Ohmachi, T. & Tokimatsu, K. Simplified method for three-dimensional dynamic analysis of embankment dams, *Proc. of the 4th International Conf. on Numerical Methods in Geomech.*, 1982, Vol. 1, pp. 411–419.
115. Ohmachi, T. & Soga, S. Practical method for dynamic interaction analysis of three-dimensional dam-foundation system, *8th World Conf. on Earthq. Engrg.*, San Francisco, Calif., 1984, Vol. 3, pp. 1065–1072.
116. Ohmachi, T. & Nakamoto. In-situ measurement of radiation damping of existing rockfill dams, *Proc. of Ninth World Conf. on Earthq. Engrg.*, 1988, Vol. VI, Tokyo-Kyoto, Japan.
117. Okamoto, S. *et al.* On the dynamical behavior of an earth dam during earthquakes, *Proc. 4th World Conf. Earthq. Engrg.*, Santiago, 1969.
118. Okamoto, S. Earthquake resistance of embankment dams, Chap. 15 in *Introduction to Earthquake Engineering*, J. Wiley & Sons, 1973, 427–490.
119. Oner, M. Estimation of the fundamental period of large earthfill dams, *Soils & Found.*, 1984, **24,** 1–10.
120. Oner, M. Shear vibration of inhomogeneous earth dams in rectangular canyons, *Soil Dyn. & Earthq. Engrg.*, 1984, **3**(1), 19–26.
121. Papadakis, C. & Wylie, E.B. Seismic shear wave propagation through earth dams, *Soils & Foundations*, 1975, **15**(2).
122. Poulos, S.J., Castro, G. & France, J.W. Procedure for liquefaction evaluation, *J. Geotech. Engrg.*, ASCE, 1985, **111**(6), 772–792.
123. Prange, B. Resonant column testing of railroad ballast, *Proc. X World Conf. Soil Mech. & Found. Engrg.*, Stockholm, III, 273–278.
124. Prato, C.A. Simplified 3D seismic analysis of embankment dams, *Proc. of Ninth World Conf. on Earthq. Engrg.*, Vol. VI, Tokyo-Kyoto, 1988, Japan.
125. Prevost, J.H. Two-surface versus multi-surface plasticity theories: a critical assessment, *International J. for Numer. & Analytical Methods in Geomech.*, 1982, **6,** 323–338.
126. Prevost, J.H. Nonlinear transient phenomena in saturated porous media, *Computer Methods in Applied Mech. & Engrg.*, 1982, **30,** 3–18.
127. Prevost, J.H., Abdel-Ghaffar, A.M. & Elgamal, A.W.M. Nonlinear hysteretic dynamic response of soil systems, *J. Engrg. Mech.*, ASCE, 1985, **111**(7), 882–897.
128. Prevost, J.H., Abdel-Ghaffar, A.M. & Lacy, S.J. Nonlinear dynamic analysis of earth dam: a comparative study, *J. Geotech. Engrg.*, 1985, **111**(7), 882–897.
129. Prevost, J.H. & Keane, C. Shear stress-strain curve generation from simple material parameters, *J. of the Geotech. Engrg. Div.*, ASCE, 1990, **116**(8), 1255–1263.
130. Richards, R., Jr., & Elms, D.G., & Budhu, M. Dynamic fluidization of soils, *J. Geotech. Engrg.*, ASCE, 1990, **116,** 740–759.
131. Richards, R., Jr. & Elms, D.G. Seismic behavior of gravity retaining walls, *J. Geotech. Engrg. Div.*, ASCE, 1979, **105,** 449–464.
132. Richart, F.E. & Wylie, E.B. Influence of dynamic soil properties on response of soil masses, *Struct. & Geotech. Mech.*, Prentice-Hall, 1975, 141–162.
133. Roesset, J. Soil amplification of earthquakes, *Numer. Methods in Geot. Engrg.*, eds. Desai & Christian, McGraw-Hill, 1977.
134. Roesset, J. & Tassoulas, J.L. Nonlinear soil-structure interaction — an overview, *Earthq. Ground Motion & Its Effects on Structures*, Appl. Mech. Div., ASCE, 1982, **53.**
135. Romo, M.P., Ayala, G., Resendiz, D. & Diaz, C.R. Response analysis of El Infiernillo and La Villita Dams, Chaps. 6 in *Performance of El Infiernillo & La Vilita Dams Including the Earthquake of March 1979*, 1980, Commission Federal de Electricidad, Mexico, 87–107.
136. Sanchez-Sesma, F.J., Chevaz-Garcia, J.F. & Bavo, M.D. Seismic response of a class of alluvial valleys for incident *SH* waves, *Bull. of Seismol. Soc. of America*, 1987, **78**(1), 83–95.
137. Sarma, S.K. Seismic stability of earth dams and embankments, *Geotechnique*, 1975, **25**(4), 743–761.
138. Sarma, S.K. Response and stability of earth dams during strong earthquakes, Paper GL-79-13, Waterways Experiment Station, Vicksburg, 1979.
139. Sarma, S.K. A simplified method for earthquake resistant design of earth dams, *Design of Dams to Resist Earthquake*, ICE, London, 1980.
140. Sarma, S.K. & Bhave, M.V. Critical acceleration versus static factor of safety in stability analysis of earth dams and embankments, *Geotechnique*, 1974, **24,** 661–665.
141. Sarma, S.K. & Barbosa, M.R. Seismic stability analyses for rockfill dams with clayey core, *Geotechnique*, 1985, **35,** 319–328.
142. Seed, B. Considerations in the earthquake design of earth and rockfill dams, *Geotechnique*, 1979, **29**(3), 215–263.
143. Seed, H.B. Stability of earth and rockfill dams during earthquakes, *Embankment-Dam Engrg.*, eds. Casagrande Vol. Hirschfeld & Poulos, J. Wiley, 1973.
144. Seed, H.B., Lee, K.L. & Idriss, I.M. An analysis of Sheffield Dam failure, *J. Soil Mech. & Found. Div.*, ASCE, 1969, **95,** SM6, 1453–1490.
145. Seed, H.B., Lee, K.L., Idriss, I.M. & Makdisi, F.I. Analysis of the slides in the San Fernando Dams during the earthquake of Feb. 9, 1971, Report No. EERC 73-2, Univ. Calif., Berkeley, 1973.
146. Seed, H.B. Lessons from the performance of earth dams during earthquakes, *Design of Dams to Resist Earthquake*, ICE, London, 1980, 251–258.
147. Seed, H.B. A method for earthquake resistant design of earth dams, *J. of the Soil Mech. & Found. Div.*, ASCE, 1966, **92,** SM1, 13–41.
148. Seed, H.B. & Martin, G.R. The seismic coefficient in earth dam design, *J. of the Soil Mech. & Found. Div.*, ASCE, 1966, **92,** SM3, 25–58.
149. Seed, H.B., Makdisi, F.I. & De Alba, P. Performance of earth dams during earthquakes, *J. of the Geotech. Engrg. Div.*, ASCE, 1978, **104,** GT7, 967–994.
150. Seed, H.B. Earthquake-resistant design of earth dams, *Seismic Design of Embankments & Caverns*, ASCE, 1983, 41–64.
151. Seed, H.B., Bray, J.D., Boulanger, W. & Seed, H.B. Seismic response of the Puddingstone and Cogswell Dams in the 1987 Whittier Narrows Earthquake, U.S.G.S. Special Publication, 1989.
152. Seed, H.B., Seed, R.B., Lai, S.S. & Khamenehpour, B. Seismic design of concrete faced rockfill dams, *Concrete Face Rockfill Dams — Design, Construction and Performance*, ASCE, 1985, 459–478.
153. Shen, C. & Chen, Y. Thirty years of research work on earthquake resistance of hydraulic structures in China, *Design of Dams to Resist Earthquake*, ICE, London, 1980, 107–114.
154. Sherard, J.L. & Cooke, J.B. Concrete-face rockfill dam: I.

Assement, and II. Design, *Journ. Geot. Engrg.*, 1987, **113**(10), 1096–1132.
155. Sherard, J.L. Upstream zone in concrete-face rockfill dams, *Concrete Face Rockfill Dams — Design, Construction and Performance*, ASCE, 1985, 618–641.
156. Simo, J.C. & Ortiz, M. A unified approach to finite deformation elastoplastic analysis based on the use of hyperelastic constitutive equations, *Computer Methods in Appl. Mech. & Engrg.*, 1985, **49**, 221–245.
157. Simo, J.C., Govindjee, J.G.K. & Hughes, T.J.R. Unconditionally convergent algorithms for non-smooth multisurface plasticity amenable to exact linearization, *Advances in Inelastic Analysis*, ASME Publication, AMD, 1987, **88,** 87–95.
158. Singh, M.P. & Khatua, T.P. Stochastic seismic stability prediction of earth dams, *Proc. Earthq. Engrg. & Soil Dyn. Spec. Conf.*, ASCE, Pasadena, II, 1978, pp. 875–889.
159. Stara-Gazetas, E. Method for inelastic response analysis of earth dams, Ph.D. Thesis, Rensselaer Polytechnic Institute, Troy, NY, 1985.
160. Takahashi, T. *et al.* Study on dynamic behavior of rockfill dams, *Proc. 6th World Conf. on Earthq. Engrg.*, New Delhi, 1977, **6,** 2238–2243.
161. Trifunac, M.D. Scattering of plane *SH* waves by a semi-cylindrical canyon, *Int. J. of Earthq. Engrg. & Struct. Dyn.*, 1972, **1**(3), 267–281.
162. Trifunac, M.D. Surface motion of a semi-cylindrical alluvial valley for incident plane *SH* waves, *Bulletin of the Seismol. Soc. of America*, 1971, **61**(6), 1755–1770.
163. Tsiatas, G. & Gazetas, G. Plane-strain and shear beam free vibration of earth dams, *Soil Dyn. & Earthq. Engrg.*, 1982, **1**.
164. Veletsos, A.S. & Tang, Y. A deterministic assessment of effects of ground motion incoherence, Tech. Report NCEER-89-0037, National Center for Earthq. Engrg. Research, SUNY, Buffalo, 1989.
165. Von Thun, J.L. General Report, Session VII, stability of slopes and earth dams under earthquakes, *Proc. 2nd Int. Conf. on Recent Advances on Geotech. Earthq. Engrg. & Soil Dynamics, St. Louis*, Vol. III, 1991.
166. Vrymoed, J.M. Dynamic FEM model of Oroville dam, *J. of the Geotech. Engrg. Div.*, ASCE, 1981, **107,** GT8, 1057–1077.
167. Vrymoed, J. Dynamic FEM model of Oroville dam, *J. Geotech. Engrg. Div.*, ASCE, 1981, **107,** GT8, 1057–1077.
168. Wong, H.L. & Jennings, P.C. Effect of canyon topography on strong ground motion, *Bulletin of the Seismol. Soc. of America*, 1975, **65,** 1239–1257.
169. Wong, H.L. & Trifunac, M.D. Surface motion of a semi-elliptical alluvial valley for incident plane *SH* waves, *Bulletin of Seismol. Soc. of America*, 1974, **64,** 1389–1408.
170. Wong, H.L. & Trifunac, M.D. Scattering of plane *SH* waves by a semi-elliptical canyon, *Int. J. Earthq. Engrg. Structural Dynamics*, 1974, **3,** 157–169.
171. Yegian, M.K., Marciano, E.A. & V.G. Integrated seismic risk analysis for earth dams, Rep. No. CE-88-15, Northeastern Univ., Boston, 1988.
172. Yiangos, A. & Prevost, J.H. Two-dimensional two-phase elasto-plastic seismic response of earth dams, Research Rep. NCEER, State Univ. of New York, Buffalo, 1991.
173. Zienkiewicz, O.C., Leung, K.H. & Hintom, E. Earth dam analysis for earthquakes: numerical solutions and constitutive relations for non-linear (damage) analysis, *Design of Dams to Resist Earthquake*, ICE, London, 1980, 141–156.
174. Zienkiewicz, O.C., Pastor, M. & Xie, Y.M. Constitutive modelling of soils and computation of earthquake damage and liquefaction, *Proc. 2nd Int. Conf. on Recent Advances in Geotech. Earthq. Engrg. & Soil Dynamics*, St. Louis, Vol. II, 1991, pp. 1743–1752.